



School of Chemistry

Pulsed Direct-Current Plasma Assisted Chemical Vapor Deposition (PDC PA-CVD); startup, optimization and its application in creation of isotopically pure diamond layers.

Dominic Richard Palubiski

This thesis is submitted in partial fulfilment of the requirements for the Honours Degree of MSci (Bsc) at the University of Bristol

Assessor: Professor Neil Fox

Second Assessor: Professor Paul May

Third Assessor: Professor David Fermin

Physical and Theoretical Group

I would like to thank Professor Fox and Professor May for their help with this project along with Dr. Smith and Mr. Bickerton for the great number of hours they spent tolerating me and helping me produce some results. Also Dr. Othman deserves mention for giving up his seeded samples for testing, along with Dr. Croot and Dr. Truscott for teaching me how to use the SEM, staying with me late into the night in doing so.

Contents

Abstract.....	4
Chapter 1: Introduction.....	4
Chapter 2: Theory of CVD diamond growth.....	6
Deposition Parameters.....	6
Analytical Analysis.....	16
Chapter 3: Pulsed Direct Current Plasma Assisted Chemical Vapor Deposition (PDC PA-CVD).....	20
Chapter 4: Experimental Plan.....	24
Taguchi Optimization.....	24
Project Plan.....	31
Issues and Modifications.....	34
Chapter 5: Experimental Results and Discussion.....	38
Chapter 6: Conclusions and Future Research.....	54
Further Research.....	56
References.....	59

Abstract

A new Pulsed Direct Current Plasma Assisted Chemical Vapor Deposition (PDC PA-CVD) instrument has been constructed and preliminary deposition runs have been done, laying the ground work for diamond deposition in the near future and a full optimization of the system shortly after. Preliminary results from OES spectrums show incredible plasma stability and uniformity, allowing for steady depositions over hours with little variation or destabilization. The primary deposition run progressed out of necessity due to shortness of time and to conserve the instrument for one complete experiment, due to the possibility of faults arising and extended down time ensuing. The results showed mostly graphitic deposition occurring although limited evidence in the form of a 1140 cm^{-1} Raman peak and possible ballas diamond 'scales' on SEM images did point towards nanocrystalline diamond growth within the mainly graphitic film. Further deposition runs were unable to grow pure diamond but upon increasing the cathode and substrate temperature to $>600\text{ }^{\circ}\text{C}$ rapid deposition was seen and a solid film was produced, showing a definite 1333 cm^{-1} shoulder on its Raman spectrum, along with ballas diamond growth and obvious film thickness on SEM images.

Non-deposition experiments have shown that the production of key CH and C_2 radicals in the plasma occur at high enough concentrations to observe on OES at methane concentrations above 4% in pure hydrogen. However, the experiments also showed that the system had an air leak, resulting in the production of CN radicals during deposition, affecting growth and deteriorating the diamond film quality. The variation of temperature across the substrate has also shown to be minimal, essential for even film deposition.

Overall the potential for high quality nanocrystalline film is evident, pure diamond deposition an expected achievement, and after optimization outlined within this report, a steady stream of high quality diamond films could be produced with minimal human input.

Chapter 1: Introduction

The University of Bristol's Diamond Laboratory^[28] has activated its new PDC-PACVD instrument this year. With this new, in-house designed and built system in operation now there will be a large number of obstacles to overcome to be able to produce diamond, and to produce these films repeatedly and reliably. The initial step would be to attain deposition conditions within the instrument, overcoming issues and faults, design miscalculations and other obstacles. To produce ideal conditions for production, extensive research was conducted into the production of diamond films. This also opened avenues of further research towards the production of high quality diamond. This research allowed for a further look into the optimization of the new instrument, with an exploration of the Taguchi method and its possible application to this specific field discussed, with the possibility of enabling a fully automated and optimized system.

Diamond has always been sought after as the best of the gem stones, but practical uses, over material looks, have been attracting greater attention over the past half century. Diamond properties are usually located at the extremes of many rankings. Diamond has the highest molar density, sound velocity, hardness, elastic module and thermal conductivity, along with the lowest compressibility, of all known materials^[86]. Currently diamond is prohibitively costly to produce or obtain. The successful commercial production of high quality diamond could lead to a revolution in both their application and in the machines that use them. Diamond has the potential for a vast range of uses^[30-33]. One example could utilize its extreme thermal conductivity, along with its low thermal expansion coefficient, for supporting ultra-high powered microwave electronic devices, with the diamond able to remove heat buildup from the Ga-N devices with no damage to the devices themselves, extending their operating ranges and life span^[87]. As diamond also shows near perfect biocompatibility, much like gold^[88], this has been exploited through the production of a base, shaped for various uses, for neuron growth in the medical community^[89]. This direction of research could lead to the regrowth of human brain sections, providing pathways to possible Alzheimer's remedies, or possibly the fabrication of a living computer. To compete against possibly living computers, diamond even has its own application; the possibility of producing quantum bits and computers^[90] itself. The list of possible applications of diamond is long, with numerous applications arising from its various other properties such as its high breakdown voltage and low dielectric constant^[48].

For the properties of diamond, and the consequent applications to be fully explored, the issues of production must be solved. A quick, reliable and inexpensive production of a range of diamond shapes, sizes and qualities needs to be found. This is what the new PDC PA-CVD instrument aims to achieve.

Overall, this project overall aims for the repeated and reliable production of high quality diamond films. To achieve these aims the new instrument must not only be constructed, with many delays and faults to overcome, but initial tests must also be done to ensure the instrument operates as planned, and achieves an optimization that allows fabrication to occur at a relatively rapid rate. The following chapters will go through the various steps taken to achieve these aims and initially will look into the theory behind diamond growth. This will give a base of a strong chemical and physical knowledge to be able to apply to the varying parameters on the new instrument, and how they will affect the overall diamond quality. Without this background, the startup of the new machine would be infinitely harder. If no knowledge of other issues and obstacles that have arisen within the general scientific community from similar instruments is understood, then these issues will be had again.

After looking at the theory behind diamond growth, this report will look at why the new PDC PA-CVD instrument is being constructed. It will look into what other CVD instruments are commercially available and what limitations they possess that the new PDC PA-CVD instrument aims to make obsolete. This will be followed by the experimental plan, laid out to allow not only for achieving

rudimentary fabrications but with the aim of optimization through the Taguchi optimization process. Setting up the initial deposition experiments with the eventual Taguchi optimization in mind allows for the deposition parameters to be calibrated for the optimization process. This will allow easy incorporation into the Taguchi method afterwards, allowing for a more effective optimization process.

The next chapter will look at what was learned from these initial experiments along with various issues and delays that were experienced during experimentation. This will allow for a qualitative analysis of the new instrument and further refinement for future work. That future work will be discussed lastly. With the experiments concluded a future plan can be constructed to allow for the eventual goal of thin films of isotopically pure diamond to be created, with minimal structure irregularity, boundary layer thickness and crystal size.

Chapter 2: Theory of CVD diamond growth

Deposition Parameters

The new instrument has a wide range of parameters that need to be taken into consideration when looking at initial fabrication runs and setup. These will be looked at in detail alongside examinations of the chemistry and physics behind diamond growth, allowing for a full understanding of areas of interest relevant to ensuring high quality diamond growth.

Gas Pressure

The pressure at which the reactor runs determines the overall concentration of reactants and usually correlates with a higher growth rate and a reduction in defects as the pressure increases^[41,17]. As the pressure increases Raman spectroscopy results show definite sharpening of the 1332 cm^{-1} diamond peak, along with a shift from spherical diamond to more cubic structures on Scanning Electron Microscopy (SEM) imagesⁱ. Further research^[52] shows that increased pressures results in smaller diamond crystal sizes, with the morphology changing from micro to nanocrystalline as the pressure increases from 40 – 300 Torr, but was conducted using a Hot Filament Chemical Vapor Deposition (HFCVD) system so may not correlate with a PDC PA-CVD system. Further research has shown a decrease in nucleation rates when pressures above 30 Torr are used^[98]. DC PA-CVD systems have been shown to increase nucleation rates relative to other fabrication methods^[1] and this may be able to be counteracted with the new system. While different applications require different exact shapes and morphologies of diamond, nanocrystalline is most sought after. The small crystal size will limit the variation in the surface layer height, allowing for minimal boundary layer overlap when multiple layers are deposited upon each other. The minimization of boundary layer will be essential as individual

ⁱ See Analytical Analysis for further information.

layers will have various isotopic, electrical, or thermal properties and to minimise the boundary zone will allow a shrinking of the individual layers, improving the produced devices efficiency.

Gas Composition

Many different gases could, in theory, be used as plasma or reaction aids, or as reagents themselves, for diamond synthesis. This is one of the most vital components of diamond fabrication. Typically hydrogen, with a hydrocarbon gas as a carbon source, is used to create the correct deposition plasma for diamond formation. Without this gas no material would be available to create the diamond. Due to graphite being chemically more stable than diamond^[97], diamond deposition occurs under non equilibrium conditions. Critical non-equilibrium must be created though both the energy introduced and ensuring the correct ratio of gasses are present. Some of the options will be explored here.

Hydrogen

Hydrogen is essential for consistent diamond growth. Hydrogen removes deposited graphitic carbon clusters up to 30 times faster than deposited diamond^[54]. The main use of hydrogens is for the stabilization of dangling bonds. As the methyl radicals are deposited on the substrate surface they will create unbound radicals at the surface of the growing diamond. Hydrogen radicals react with these and help to cement the carbon into its sp^3 configuration, that of diamond (**Figure 1 (a.)**)^[55]. sp^2 hybridized carbon, *i.e.* graphite, is also deposited^[16] so as deposition is progressing both diamond and graphite are formed (**Figure 1 (b.) & (c.)** respectively). To ensure that the final product has as few impurities as possible the rates of removal of both deposits is critical. Hydrogen removes the graphite before it is encased in further deposits, such as further graphite or diamond growth. If deposited in diamond then removal will not occur, as diamond growth is preferred over diamond removal, and permanent quality

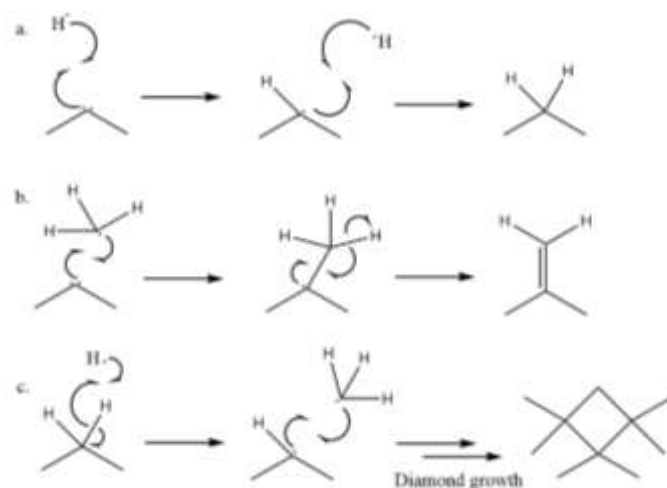


Figure 1. The three main reactions involved in diamond synthesis. Reaction a; the addition of atomic hydrogen allows for the protection of exposed sp^3 carbons. If the level of hydrogen is too low then, after initial carbon addition, further methyl radicals will react, leading to sp^2 bond formation and the eventual production of graphite (b.). The hydrogens can then be removed to allow further carbon addition, the rate of which can be controlled through the hydrogen concentration (c.).

degradation will occur. The reverse of reaction (b.) progresses at a much faster rate, roughly 20-30 times faster^[93], than the reverse of reaction (c.), allowing the quicker removal of graphite relative to diamond, producing a higher quality final diamond.

This stabilization reaction is in a dynamic equilibrium, constantly removing and adding hydrogens to the surface of the forming diamond film. The removal of a hydrogen, with the addition of a methyl

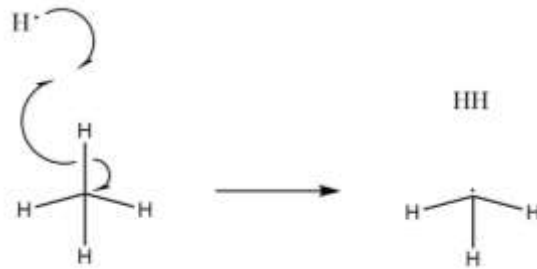


Figure 2. Reaction mechanism for the production of methyl radicals from methane.

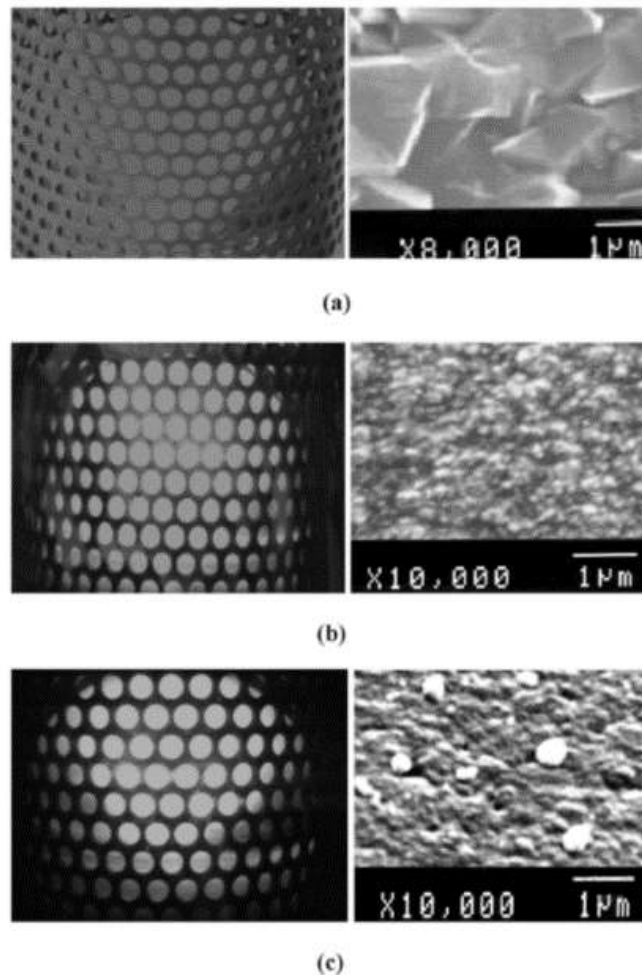


Figure 3. ‘Appearance of plasmas (left; see web version of this paper for color photos) and the resulted surface morphologies. SEM images (a) microcrystalline diamond film (2% CH₄ + 98% H₂, 1.2 kW, 51 Torr, 125 sccm, 900 °C), (b) nanocrystalline diamond film (1% CH₄ + 5% H₂ + 94% Ar, 1 kW, 175 Torr, 30 sccm, 700 °C) and (c) nanocrystalline diamond film with some sub-micron particles deposited by an unstable plasma (1% CH₄ + 99% Ar, 550 W, 200 Torr, 5 sccm, 550 °C).’ [16]

radical over another hydrogen, allows for the growth of the diamond film. Care must be taken to ensure the concentration does not increase to the point where the rate of reaction suffers. If the removal of formed diamond becomes greater than deposition, the growth of the diamond is halted and the quality is negatively affected. In contrast, a concentration that is too low results in the inadequate removal of graphite and will result in carbon clusters forming. There is a narrow operational range to ensure the correct concentration is achieved and growth occurs.

The benefits of hydrogen also include the reduction of the critical nucleus^[56]. This aids growth and the formation of diamond by reducing the number of carbons that need to group together to produce a stable diamond nucleus.

Atomic hydrogen, from hydrogen gas, is easier to produce than methyl radicals from methane. But hydrogen pushes this reaction to the right hand side of the reaction, as shown in **Figure 2**, allowing the greatest growth radical, CH_3 , to be formed in much greater numbers through the reaction diagrammed above^[56], although some debate remains about its key role in the process. The hydrogen also helps to stabilize the plasma allowing for steadier and increased deposition^[16]. Without the stabilization, the reactor produces single nanodiamonds as well as a general low quality film, as shown in **Figure 3**.

Argon

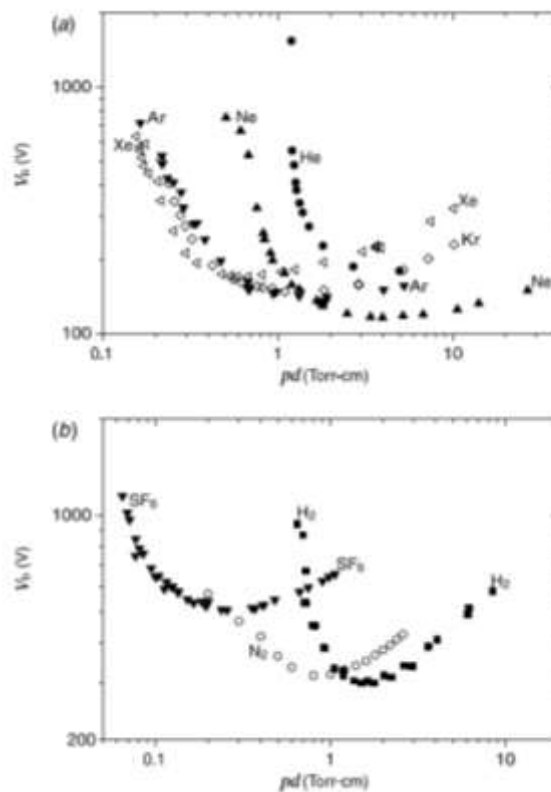


Figure 4. 'Breakdown voltage for plane-parallel electrodes at 20 °C: (a) noble gases; (b) molecular gases (data supplied by Petrovic and Maric, 2004).' [58]

Argon is used traditionally as a plasma initiator and stabilizer gas due to its low ionization energy relative to hydrogen and methane^[57,58]. As the plots known as Paschen curves shown in **Figure 4** show, the breakdown voltage for argon is over 150 V lower at 1 Torr than hydrogen. This reduces the power requirements needed to form a plasma and, as an inert gas, is safe to use without risk of chemical reactivity. The low ionization energy also produces a plasma that is more tolerant to variations in power or current.

Argon has been shown to improve the rate of deposition of diamond films^[51,62] and has been shown to shift produced diamond from microcrystalline to nanocrystalline morphology^[16] (**Figure 3**) when added to reaction mixtures. This, however, leads to increased deposition of graphite-like carbon clusters^[51]. Since the aim of the new reactor is to produce higher quality diamond, regardless of the cost of production times, this is a non-ideal effect of argon. Small quantities of argon may be experimented with to aid growth rates if exceptional diamond is grown under more favorable conditions, but not for initial calibration.

Methane

Diamond growth requires the addition of a single carbon molecule in a sp^3 configuration onto the preexisting diamond surface. There are many different feed gases to be considered that could potentially be used to achieve this, but methane gas is the most viable option. The major factor in the suitability of a feed gas is its quality of being a gas at room temperature. This makes it easy to use and easily ionized. Also, its effectiveness in contributing to the production of high quality diamond is critical. While methane was chosen as the ideal gas, many other options have been experimented with.

Any alkane chain longer than butane can be disregarded as they are liquid at room temperature and therefore unsuitable for use in diamond growth. Chains shorter than butane but longer than methane can also be disregarded as single carbon addition onto a growing diamond surface is preferable to chain addition. For example, if propane is added to the existing diamond structure a single carbon binds to the existing diamond surface, then the unbound chain carbons do not adopt a standard conformer, resulting in non-standard addition and a loss in the structural regularity of the diamond and therefore overall quality due to the production of lattice defects and hillocks.

Ethyne has been experimented with as a feed stock gas. But longer chains of the alkyne series, such as propyne and butyne, have not been used because of them being a liquid at room temperature, leading to issues with introducing them into the deposition environment. Ethyne has the advantage of producing the C_2 radical most easily, often seen in Optical Emissions Spectroscopy (OES)ⁱⁱ of plasma gases^[10]. This radical is linked directly to the concentration of the methyl radical which, in turn has shown to increase the quality of diamond produced through steady reliable addition of sp^3 carbons onto the

ⁱⁱ See Analytical Analysis for further details.

lattice. Further research has shown, however, that ethyne's rate of incorporation is much slower than that of methane through both carbon 13 based experiments^[14] and physical growth experiments^[13,15]. The methyl radical is thought to be the reason behind this and is postulated to be the main growth species over the C₂ radical. This radical is more easily produced from methane than from ethyne. C₂ radicals are seen in both methane and ethyne reaction spectra as shown in the reaction chart^[14] below (**Figure 5**):

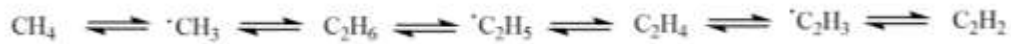


Figure 5. Reaction pathway for methane/ethyne interconversion within plasma systems. The molecules react with atomic hydrogen in similar fashion to the reaction in **Figure 2**.

Other Gases

Other trace quantities of gases may be used to aid the development of diamond growth. Various experiments have been conducted with other gasses but there has been limited success.

Oxygen has shown some success. Several papers document the use of the addition of oxygen to a reaction chamber and show that with small additions of oxygen containing molecules (i.e. CO, O₂, or CH₃OH) at concentrations less than ~0.25%, an increase in growth rate is observed. Any higher concentrations and a rapid drop in growth rate is observed^[51,64]. This is due to oxygen acting in a similar way to hydrogen (**Figure 1**) as it removes terminating hydrogens to allow further diamond growth. But at concentrations that are too high, the rate of removal is higher than the rate of deposition producing uneven and poor quality growth, or, in extreme cases, oxidizing the surface of the diamond. Both of which greatly deteriorate the diamond quality. Through the formation of OH radicals under certain conditions, oxygen can have the beneficial effect of removing formed graphite-like layers, but this has to be carefully balanced with its tendency to oxidize the surface if any benefits are to be shown.

Oxygen is useful for producing good quality diamond at substantially lower than usual temperatures (<500 °C)^[62], but with both a sharp drop in the growth rate as the temperature dropped^[62,64] and the aim of running the new reactor at higher than normal temperatures (>1100 °C), which is linked to greater oxygen etching and oxidation, this path of research is not ideal for the current set up. However, with oxygen allowing the formation of diamond in otherwise impossible conditions, such as at low temperatures or high methane concentrations, further research is potentially worthwhile after the initial instrument calibration has been completed.

Chlorine has also been investigated for its effects on growth species concentrations and product quality with little benefit^[59] observed. When tested in a methane/hydrogen plasma and the concentration of chlorine is above 4% then a rapid deterioration of the diamond film quality is observed. No major benefits are seen below 3% chlorine concentration with a small percentage incorporated into the diamond surface morphology but no other notable differences in structure or quality of the film. Furthermore metal from the reactor chamber and deposition plate was found in trace quantities in the

produced diamond; chlorine atoms become HCl upon incorporating into the plasma system. This has a corroding effect on any metal, and possibly other materials, within the reactor, so should be avoided at all costs.

Nitrogen is present in all natural diamond and is the main impurity found within all diamond. Nitrogen's molybdenum phase diagram^[66] shows definite reactions with the metal at deposition conditions with experiments^[50] showing deposits on the molybdenum cathodes, reducing their effectiveness and causing molybdenum addition to the diamond, reducing its quality. With CVD diamond grown under reduced atmosphere, where leaks are hard to remove completely, trace quantities of nitrogen are usually present in the reaction chamber. While research has been undertaken into how nitrogen becomes incorporated through leaks and its effects^[60], intentional addition of nitrogen has shown to be very detrimental to diamond film growth^[61,11] and measures should be put in place to remove it from the deposition reaction.

Methane Concentration

The percentage concentration of methane shows definite zeniths in relation to growth rate in almost any deposition set up^[49,51,64], with some showing purely increasing rates of growth as the concentration increases, albeit with increasing errors and limited data^[7]. While an increase in the concentration of methane past its zenith usually reduces the overall growth rate, it also produces other unwanted side effects such as an imbalance in the diamond growth rate; with the center growing at a slower rate than the edges of the film^[49]. This is thought to be due to the shape of the plasma as it is altered greatly through different methane concentrations (**Figure 6**). The shape of the plasma needs to be monitored to ensure its uniformity during depositions to ensure a regular diamond layer is produced. This allows for a quick and easy way of predicting the viability of the current experimental set up, in relation to the quality of diamond to be produced, based on the plasma shape and colorⁱⁱⁱ. An increase in growth rate is usually coupled with a deterioration in diamond quality. This balances production speed with film quality for eventual production depositions. While these issues are not evident with other forms of CVD diamond synthesis, the manifestation of them in other DC PA-CVD papers has shown them to be a new consideration for fabrication.

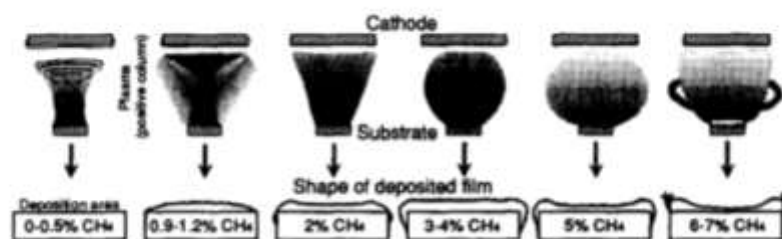


Figure 6. 'Relation between plasma appearance and diamond thick film shape as a function of the concentration of methane.' [49]

ⁱⁱⁱ See Analytical Analysis for further details on plasma color.

Considering the range of concentrations of gases for diamond growth, Bachmann *et al.*^[94] constructed a phase diagram for C-H-O combination deposition systems. This phase diagram shows areas of diamond growth, graphitic growth, and also conditions unfavorable for any growth. While the addition of oxygen has not been incorporated in the current instrument configuration, and the benefits are known to be limited, the oxygen absent line (the C-H axis) was examined for possibilities of diamond growth. Unfortunately the range of carbon percentages for growth on the Bachmann diagram, 0.002-0.023%, were much lower than those reported on papers utilizing similar systems to the PDC PA-CVD system being installed, ranging from 0.059-0.116% carbon^{iv}. While the percentages themselves may not be of significant importance, a similar diagram could be constructed for the new instrument for future diamond fabrication, including the various forms of diamond fabricated (ballas, nanocrystalline, single crystal etc.). Further discussion of other elements of the Bachmann phase diagram will be considered throughout this paper.

Argon or Hydrogen Rich Reaction

Two main environments for deposition are commonly used for CVD. Argon rich refers to an atmosphere that is constituted of a majority of argon, usually >80% argon, while hydrogen rich is mainly constituted of hydrogen, again >80% hydrogen. With limited data comparing the two, although current data can be used as a starting point, full experiments have to be conducted to provide a valid comparison. Liu *et al.*^[16] showed vast changes in composition between argon rich and hydrogen rich environments (**Figure 3**). With direct swap for argon with hydrogen, and only 1% methane as the remainder of the environment, the produced film does go from micro to nanocrystalline diamond, but with a greater instability of the plasma and many sub-micron particles across the diamond. Upon the addition of a small percentage of hydrogen, 5%, these deposits, and the plasma instability, disappear and only nanocrystalline diamond is left. Another paper^[51] shows a rapid decrease in growth rate, and a change in morphology of the produced diamond as the argon concentration passes ~30% and follows up to 99%. Further experiments^[51] showed an inherent instability in the argon rich plasma compared to a standard hydrogen rich environment on a DC PA-CVD machine. The heavy argon atoms were thought to be kinetically too powerful for the molybdenum cathode, leading to sputtering, incorporation of Mo-C centers in the diamond and a non-uniform diamond product. But other research has been able to rectify this issue through addition of the argon only after full reaction pressure is obtained in a hydrogen rich atmosphere and a plasma has been struck^[65]. With the use of a molybdenum cathode and substrate, along with the similarities in set ups between the different machines, the difficulties in preparing a successful argon rich plasma will be hard to overcome, making a hydrogen rich atmosphere a much more time efficient approach.

^{iv} 2% methane to 5% methane.

Substrate/Cathode Temperature

The effect of substrate or cathode temperature on the quality of diamond produced is not very well documented in the literature. One paper utilizing a PDC PA-CVD^[49] stated that a range between 900-1000 °C was critical for diamond formation, any lower caused carbon deposits to form, while any higher and the molybdenum becomes heavily carburized. But this finding is in stark contradiction to another paper, which ran samples in non-pulsed DC PACVD, running as high as 1300 °C^[6] or as low as 800 °C^[50]. Since both of these papers reported outstanding results it appears each instruments specific parameters results in a specific set of tolerances.

Other papers have shown that as the temperature increased there was a greater tendency for microcrystalline films to be developed, as opposed to nanocrystalline^[52]. This could reduce the quality of the diamond films produced but if extrapolated could suggest single diamond formation at extremely high temperatures. Chae *et al.*^[7] showed a loose correlation with temperature and substrate growth. Their results shows an increase in the growth rate of the center of the diamond film, from $\sim 7 \mu\text{m h}^{-1}$ to $\sim 10.5 \mu\text{m h}^{-1}$, as the substrate temperature rises from $\sim 1130 \text{ }^\circ\text{C}$ up to $\sim 1240 \text{ }^\circ\text{C}$, meanwhile the edge growth rate decreased from $\sim 12.8 \mu\text{m h}^{-1}$ to $\sim 11.5 \mu\text{m h}^{-1}$ over the same temperature range. This shows that a more homogenous plasma is being produced as the edge growth rates converge, allowing the production of a more even film. This, along with Chae *et al.*'s results of a 'uniform and homogenous'^[7] disk produced, give merit to the prediction of improved diamond formation at higher temperatures. This is contrasted with other papers^[94] which show that as the temperature increases a decrease in the range of concentrations is seen. Eventually a complete loss of any possible concentrations of methane for diamond fabrication is observed when conducting experiments at higher temperatures. While the quality of diamond produced was not commented on this should be taken into consideration when conducting higher temperature experiments. As the fabrication windows shrinks, it becomes increasingly more challenging to produce quality diamond at higher temperatures and greater precision must be taken to ensure the range is found.

Exact temperature limits on the new PDC PA-CVD instrument have yet to be fully tested and will have to be based on the effectiveness of the instruments water cooling and thermal conductivity of the cooper spacers behind the molybdenum plates^v. The cathode and substrate were both chosen to be molybdenum because of molybdenum's very high melting point of 2623 °C, in theory allowing experiments to run near this temperature. A copper spacer was used to allow for optimum electrical and thermal conduction between the cathode/substrate and the input voltage feedthroughs', but with its melting point of just 1084 °C the thermal limits of the instrument is restricted to copper's limits. As seen in **Figure 10**, the water-cooling is placed directly behind the copper plate, and a thermocouple is placed between the copper and the molybdenum plates. Diagnostic runs will have to be done to ensure the temperature can

^v See Chapter 3 for more information.

be properly maintained. When the temperature of the thermocouples can be stabilized at around 800 °C then pyrometers can be used to determine the actual substrate and cathode temperatures for further testing.

Plate Distance and Setup

The majority of set ups discussed in available literature only documented a single plate distance, because they are generally focusing on other parameters. One paper however produced a set up allowing for the interelectrode distance to be reduced to 5 mm^[50]. While the results from the initial distance to this distance were not documented, the paper reported that upon reaching 5 mm the plasma column was eliminated and only the faraday dark space (described in [53]) remained. This led to the postulation that the electrons, uninterrupted by the plasma, were producing the exceptional diamond through high energy bombardment. With the current instrument set up it may be possible to explore this further in the hope of replicating the quality of diamond reported.

The standard interelectrode distance is generally accepted to be a few centimeters^[2,7,49], although most papers failed to report the distance used in their set up. An electrode gap of a few centimeters has been used as the standard for the instrument with the aim of replicating the more standard/homogenous results. No research could be found on the effects of interelectrode distance and diamond quality in PDC PA-CVD instruments. Further research needs to be done to understand specifically the effects with relation to this specific PDC PA-CVD instrument.

Deposition Times

Deposition times vary greatly between papers^[6,7,49,50] but show little effect on the quality of the produced diamond. Further tests^[43] utilizing Raman Spectroscopy show little alteration in the Raman linewidth, reflecting the quality of the produced diamond, over deposition times of up to 72 hours. Because of the high temperatures of fabrication used, diamond become conductive enough to allow the plasma to be maintained. Extreme thicknesses may halt deposition but no literature papers have tested this to its extremes due to the excessive growth times needed (greater than 4 or 5 days), although this also depends significantly on the growth rate itself.

Power

The power supply of the new instrument produced power at a maximum of 10 kW, with voltage and current limits stated in **Table 2**. The closest instrument set up, produced by Lux *et al.*^[49] utilized a power of 3.6 kW, 800 V at 4.5 A through a PDC PA-CVD system. Feedthrough issues have limited the voltage ability of the instrument^{vi} so exact replication of the conditions had to be halted. Similar, but not exact 3.6 kW conditions can be replicated using ~300 V and ~12 A, This should produce similar effects. Other main DC PACVD systems utilized power levels well above the capabilities of the current set up, with

^{vi} See Chapter 3 for further details.

some reaching as high as 50 kW^[7]. As a result of this, combined with their lack of a pulse set up in their deposition runs (see next section), there is only one paper providing relevant power levels for depositions runs. This paper^[49] only conducted deposition with power levels ranging between 3.5-3.8 kW and no other literature data found on the effect of diamond growth rate or quality with a variation in power levels. Therefore the majority of experiments will have to be done with limited background knowledge, with extra focus on this area to observe and analyze all results.

Pulse Rate

Limited literature data on PDC PA-CVD systems exist, and with varied instruments specifications the results of these experiments cannot be directly correlated. The closest experimental set up to the current instrument used a pulse rate of ~45 kHz^[49]. This produced high quality diamond but no comparisons to different pulse rates were presented. Other research has used a frequency of between 100-200 kHz with a positive pulse duration of 2016 ns^[18]. This showed improvement in diamond quality, based on friction, wear resistance, stress and roughness, over standard radio frequency CVD, but again experimented little with the effects of growth of diamond quality with a variation in pulse frequency. What can be tentatively taken from the difference between the pulsed and non-pulsed papers is the levels of power needed for fabrication. While a wide variety of factors could lead to these discrepancies, including the variations in the set up and the size of the deposition areas, the pulses systems use a lot less power, 3.6 kW^[49] vs 20 kW^[50], to produce their respective diamond films.

Analytical Analysis

Once the production of the diamond has been completed a more robust analysis of the film has to be done to quantify variations in the quality. While many different analytical techniques have been developed, three main ones are of most use in the characterization of diamond films, one for production, the other two for product analysis. Optical Emissions Spectroscopy has the ability to probe the production of the diamond films through viewing the chemical species in the plasma identifying exact growth conditions, and understand how changing conditions alter the chemical fabrication process. Scanning Electron Microscopy and Raman Spectroscopy allow, non-invasively, examination of the surface structure and the internal structure respectively, showing not only the morphology of the film but also purity and type of diamond formed.

Optical Emissions Spectroscopy (OES)

Used for non-invasive analysis of deposition plasmas, OES provides identification of various molecules and radicals within the system, allowing for both a comparison of conditions between experiments, and an insight to the possible chemical reactions occurring during fabrication.

Within the high energy plasma molecules' electrons are constantly jumping between energy levels and emitting photons corresponding to those energy levels gap. Since each molecule and radical species

produces different energy photons from their individual energy gaps, varying species have been identified and identification of a standard plasma composition has become routine. The advantage of using OES to monitor diamond fabrication is that simply by pointing the fiber optic bundle through the viewing window during fabrication one can assess the possible outcomes of the experiment. This comes from work of Balestrino *et al.*^[70] showing the variation of CH and C₂ radicals within the plasma, and the effects on the quality of diamond produced. With an increase of the C₂ radical the quality of the diamond film decreases and the instances of graphite-like carbon increase, reflected in the Raman spectra. Because of the various wavelengths emitted from carbon, hydrogen, argon and oxygen species identifiable to their various states (CH, C₂, H_α, etc.)^[9-11], quick identification becomes straightforward. However, further analysis of exact growth conditions and reactions requires further research and extensive analysis, which is beyond the scope of this paper. An Ocean Optics USB2000 UV-Vis ES^[75] instrument was used for all OES measurements taken in this paper. While detailed characterization could not be done with this instrument, this was beyond the scope of the experiment and also was non-essential for initial characterization of the new PDC PA-CVD plasma system.

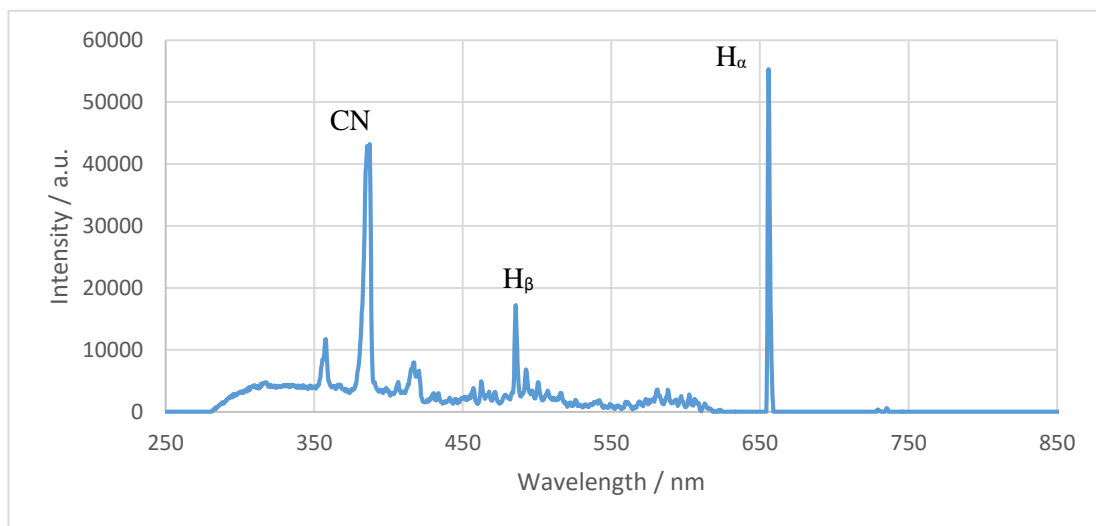


Figure 7. OES spectrum of deposition experiment 1 (4% methane in hydrogen, 87 ± 13 Torr, 4.75 kW, 100 kHz) with some of the main peaks noted.

Scanning Electron Microscope (SEM)

With the limits of resolution based on the size of the wavelength of the optical medium, which traditionally has been visible light (~ 550 nm), the best images are produced from features on micrometer ranges. Electron Microscopy allows for greater resolution due to smaller wavelength electron beams (~ 10 pm). This can produce images with resolution on the nanometer range allowing for greater detail on images of surface structure (**Figure 8**). Scanning Electron Microscopy uses magnetically focused electron beams to raster across a surface, collecting the reflected beams and producing detailed images of its surface structure^[71].

Determining and classifying diamond surface structure, into single crystal, microcrystalline, nanocrystalline etc., is impossible beyond a single crystal state without utilizing SEM. Because of the

ability to view the surface and measure individual diamond crystal sizes the quality of the diamond can be better understood and classified according to its success. Almost every paper written on diamond fabrication provides a SEM image of their produced diamond^[2,7,16,49,50]. SEM's non-destructive methods combined with quick set up and ease of use allows results to be collected as soon as the film has been created. The analysis requires little time and provides quick results on the quality and regularity of the diamond films.

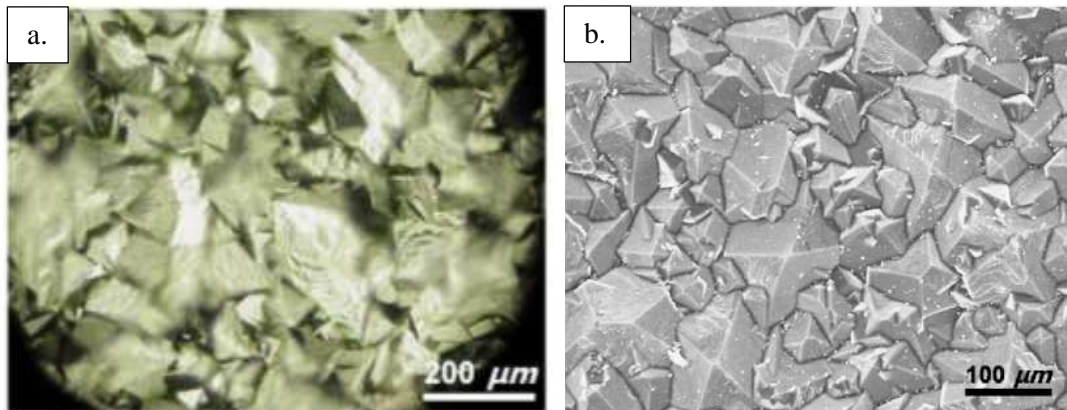


Figure 8. Optical microscope image (a.) and a SEM image (b.) of the same diamond surface, showing the variation in focal length and magnification. [7]

The most common, and ideal, diamond structure consists of regular squares of diamond (**Figure 8**), and the smaller the individual crystal size the greater the preference. As the size decreases from micro to nanocrystalline the limits of SEM resolution are approached, resulting in a loss of the exact diamond morphology. It is still useful for general crystal size and as an insight into the growth parameters of the produced film.^[16(fig.3),62(fig.4)] With unfavorable growth conditions it allows the viewing of defect structures such as pits^[61(fig.2b)], ballas shaped diamond growth^[59(fig.2d)], or single nanodiamond^[16(fig.3c)]. These different structures allow an analysis of the various growth parameters leading to their formation. This in turn provides information on how the varying deposition conditions affect the diamond film beyond simple diamond regularity, from Raman Spectroscopy, or growth rate. These techniques can therefore be used in conjunction with OES to allow a fuller understanding of the chemical reactions and conditions leading to each individual reaction mechanism.

A Jeol JSM-IT300LV Versatile Research SEM^[95] was used for imaging all produced films in this paper.

Raman Spectroscopy

Raman Spectroscopy is used to observe vibrational and rotational energies of molecules to produce 'fingerprints' of said molecules. This allows for easy characterization of a substance by comparing it against other figures to gain an immediate result with minimal sample preparation and no sample destruction^[68]. From this we can make observations of the internal structure of diamond.

Intense monochromatic light is shone onto a sample which promotes an electron to a virtual energy state. This electron then immediately relaxes and releases a photon, which is then detected at a certain

frequency. Due to the forbidden nature of this electron transition the probability of this happening is very small so the intensity of the light must be very high to enable any observable results to be measured. While this method has several issues with both the limits of light absorption and sample degradation, diamond is an ideal material for Raman Spectroscopy due to its large matrix of theoretically identical bonds, producing a sharp easily identifiable peak at 1333.7 cm^{-1} ^[43] (**Figure 9**), and no degradation of its giant covalent structure.^[67] The mixture of sp^3 , sp^2 and sp^1 bonds frequencies seen in carbon allotropes all have an energy gap of 0-5.5 eV, residing in the Raman spectroscopy IR to UV light range, allowing the imaging of all forms of produced carbon with ease^[69].

The frequency of the emitted light is dependent on the ground state energy level of the bonds being examined. When impurities are introduced into the system they alter the bond's energy levels and result in a shift in the frequency. Through this effect one can identify and, using relative intensities, calculate the concentrations of these impurities within the grown film. With peaks for amorphous graphite-like carbon well documented^[15,41,43,69], with frequencies of $\sim 1450 \text{ cm}^{-1}$, the relative construction of the diamond can be assessed with ease. With the addition of carbon 13, and the alteration of the bond's vibrational frequency though the increase in the carbons mass, it is possible to measure the relative concentrations of carbon 13 to carbon 12. The shift has been documented in a papers^[14] and allows for 0.1% concentration determination between $^{13}\text{C}/^{12}\text{C}$ ratios. With a linear shift, the Raman frequency of diamond moves from 1333.7 cm^{-1} at 1.1% ^{13}C ^{vii} over to $\sim 1280 \text{ cm}^{-1}$ at 99.3% ^{13}C . When individual layers of carbon-13 and carbon-12 diamond begin to be synthesized on the new PDC PA-CVD instrument, this technique will be able to produce information on the size and roughness of the boundary layer. This will allow for the reduction of the diamond layers to a minimum thickness eliminating the need for trial and error studies. All Raman spectrums used for this project were taken on a Renishaw 2000 Laser Raman Spectrometer^[96] at 514 nm excitation wavelength.

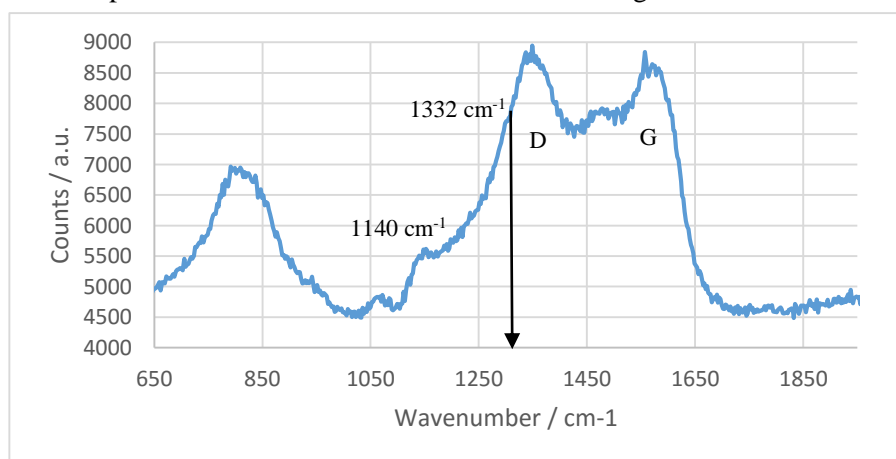


Figure 9. Raman spectrum of Experiment 4's deposition film upon the seeded molybdenum plate substrate SMo4. The relevant peaks are labeled according to the species they represent. The 1140 cm^{-1} is a surface feature of CVD fabricated diamond, and is evident within nanocrystalline diamond Raman spectrum due to the large surface area. 1132 cm^{-1} is seen for pure diamond, but not evident on this spectrum. D and G represent the disordered and graphitic bands of graphite's Raman spectrum centered around 1450 cm^{-1} .

^{vii} Natural level of the carbon 13 isotope.

Chapter 3: Pulsed Direct Current Plasma Assisted Chemical Vapor Deposition (PDC PA-CVD)

Because the extreme properties found in diamond make it suitable for a wide range of applications, there has been an increase of scientific research since initial experiments in the 1970's and '80's with a multitude of different methods for production developed. From early work with Hot Filament CVD (HFCVD)^[39,40,42] and Microwave Plasma Assisted CVD (MPACVD)^[44-46], to less well studied Electron Assisted CVD (EACVD)^[38] or Radio Frequency Plasma Assisted CVD (RF PA-CVD)^[47]; they all have their advantages but with the aim of producing high quality diamond films of large sizes, quickly, PDC PA-CVD is becoming the most appealing option for mass production, hence its choice for the new reactor.

The most widely used, and also the oldest, system in industry is the HFCVD system. The core is a heated wire filament, made of a high melting point metal such as tungsten, which is resistively heated to a high temperature with sufficient energy to dissociate molecular hydrogen into atomic hydrogen upon contact, allowing the formation of diamond. While these filaments can easily be pointed at and shaped into any surfaces shape and dimension for production, the limits of the filament themselves restrict deposition rates by limiting the allowed upper limit on the pressure for deposition; too high pressures and the filament will erode away too quickly. Heat based surface evaporation of the filaments also deposit filament material into the produced diamond, lowering its quality.

MPACVD and RF PA-CVD systems remove the issues associated with the filament by producing frequencies of energy sufficient to dissociate dihydrogen. While this allows for much higher pressures, and therefore higher growth rates, to be achieved, the electromagnetic waves are focused to a single point to make them efficient enough for use, but limits the plasma to a small confined area, reducing deposition areas greatly. Even the larger system produced by Seki-ASTeX^[91] can only expand the operation range up to about 5 cm in diameter.

These short falls are what the PDC PA-CVD system will be fixing. Electron bombardment (in a similar fashion to EACVD systems) caused by the potential difference between two metal plates, produces atomic hydrogens^[92], allowing for the formation of methyl radicals and diamond fabrication. This means that the plasma production area, and therefore the area that can be deposited on, is in theory limitless. This allows for much larger fabrication sizes and combined with the ability to run at higher pressures, like a MPACVD system, ensures that growth rates are not negatively affected. These advantages provide a key gateway to industrial growth of diamond films. A more detailed view of the instrument internals are discussed below.

Instrument Set Up

The new instrument consists of the reactor, including the low pressure, water cooled, deposition chamber and the internal deposition instruments, and the deposition environment control devices (ECD), constituting the vacuum pump, the water cooling system, the mass flow controllers, the pressure control system and the high power system.

The reactor's deposition area currently constitutes of two parallel molybdenum plates, one acting as the substrate (76 mm diameter, 3 mm thickness, grounded, **E**) and the other as the cathode (152.4 mm, 3 mm thickness, live cathode, **C**), are placed ~6 mm apart (**D**) with copper spaces (76 and 152.4 mm diameter for bottom (**F**) and top (**B**) plates respectively, 3 mm thickness) behind them. The bottom plate is placed on a water cooled plate (76 mm diameter, **G**) while the top plate is held with ~7 stainless steel clips onto the top water cooled plate (152.4 mm diameter, **A**). Deionized water was circulated and chilled through both plates and the reactor chamber walls ($>18 \text{ MOhm cm}^{-1}$, 10-12 °C). The top plate was isolated from the grounded surroundings by placing it on ceramic lifters (**H**) and insulating the copper feed through pipes in ceramic inlets. Both the current and the water cooling were fed through the copper pipes. Plate distance adjustability was inbuilt through the use of screws for plate alignment and flexible joiners to the inlet pipes to allow the variation with plate distance to be examined. The reaction gases were introduced through a ringed grounded pipe (**I**). (**Figure 10**)

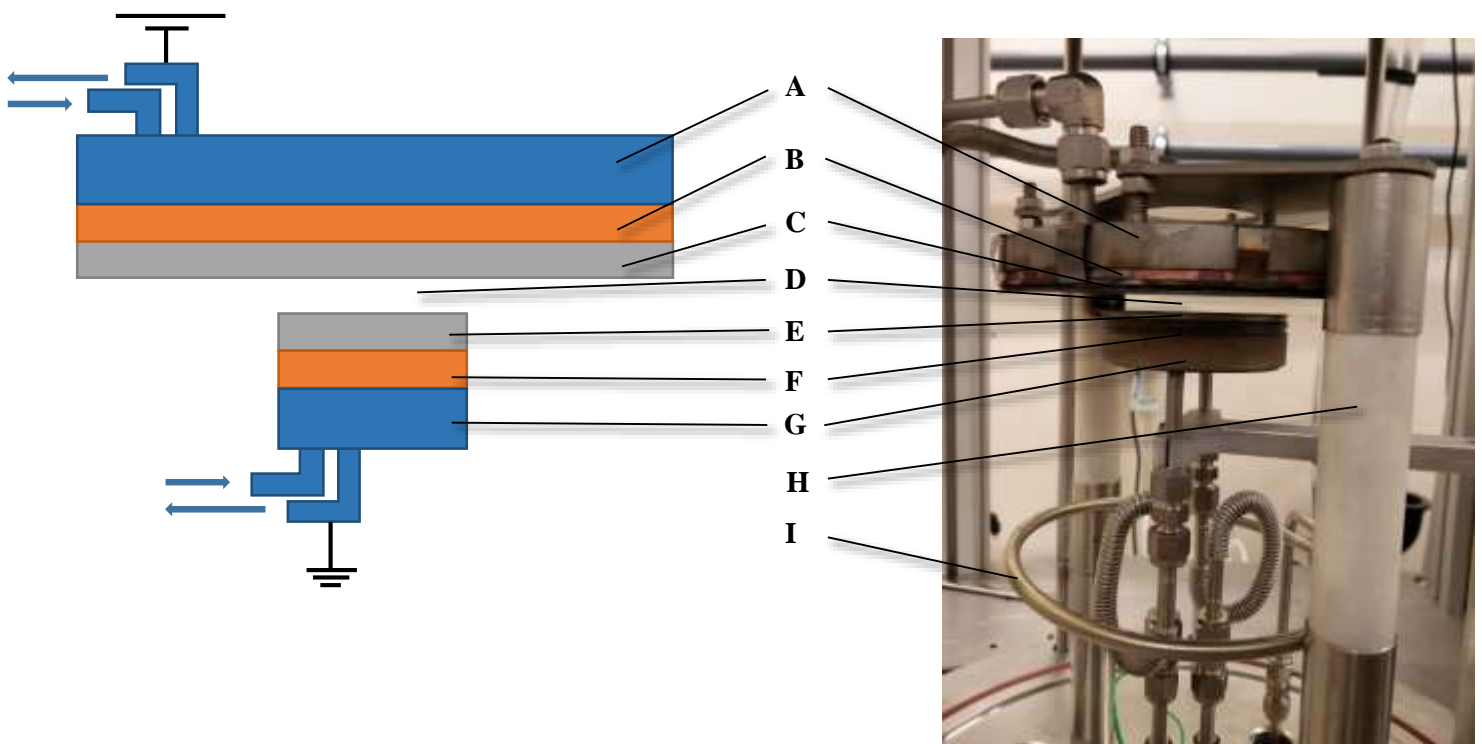


Figure 10. PDC PA-CVD reactor internals; schematic on the left, picture on the right. See text for full description.

The entire system is placed within a water cooled jacket (305 mm internal diameter, 356 mm external diameter, 610 mm height with 305 mm internal diameter rounded top.) cooled on the same connected

water cooling system (see ECD below) and grounded with the bottom plate. A viewing window of Kodial glass^[80] was installed to limit exposure to UV radiation from the produced plasma.

The ECD's main component is the deposition chamber. The chambers environment within was controlled using several systems all regulated through in-house designed software. The individual unit models used on the PDC PA-CVD instrument are listed in **Table 1**, while the limits of the system are described in **Table 2**. Full instrument schematic can be seen in **Figure 11**.

Table 1. Component model and numbers for all pieces of the PDC PA-CVD instrument.

PDC PA-CVD system	Component model
Power Supply	Advanced Energy DC Pinnacle Plus
Vacuum Pump	Edwards RV12 w/h Oil Mist Filter EMF 20
Vacuum pump valve control	MKS TYPE 252A Exhaust Valve Controller
Mass Flow Controllers	Burket Type 8715 MFC for Gases

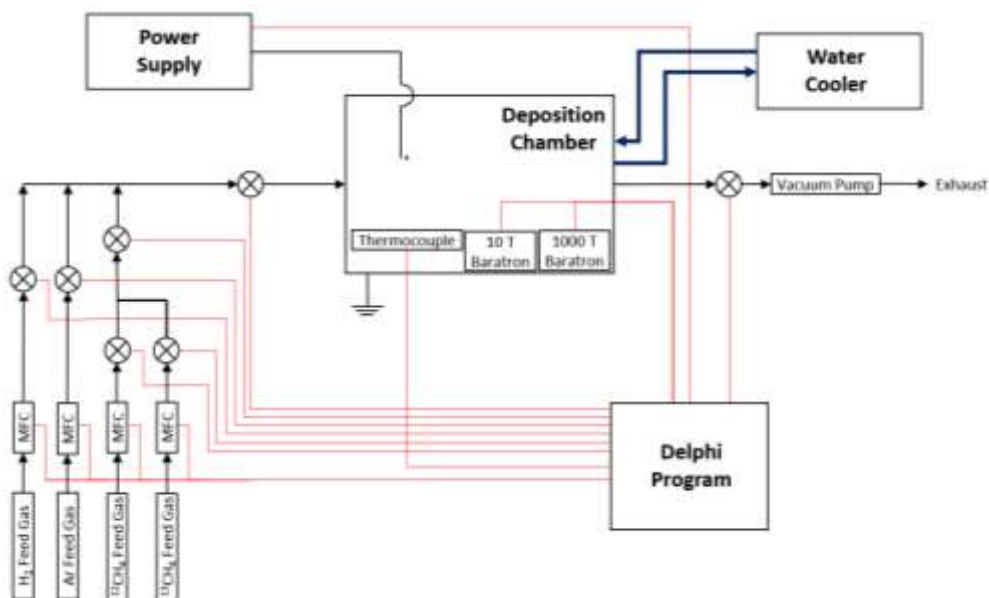


Figure 11. Schematic drawing of the PDC PA-CVD instrument. Red lines indicate a computer controlled connection, while blue lines represent water flow.

Table 2. Specification of instrument parameters.

Specification	Power	Voltage	Amps	Cathode Temperature	Substrate Temperature	Hydrogen Flow Rate	Methane Flow Rate	Argon Flow Rate
Maximum	10 kW ^b	650 V ^b	30.80 A ^b	~600 °C ^a	850 °C ^a	500 sccm	50 sccm	200 sccm
Minimum	0 W	0 V	0 A	0 °C	0 °C	0 sccm	0 sccm	0 sccm

Specification	Pressure	Plate Separation	Water Cooling Temperature ^c
Maximum	760 Torr	~50 mm	12 °C
Minimum	0.05 Torr	~1 mm	10 °C

a. Maximum temperatures currently achieved, higher temperatures expected but not under current configuration.

b. Instrument run in either power, current, or voltage limited mode. The limits of each are that modes limit, not the overall limit of all settings (i.e 10 kW will have a limit of 15.38 A if run at 650 V.).

c. This is the cycled temperature through the chiller, not the produced temperatures during deposition.

Chapter 4: Experimental Plan

Taguchi Optimization

Because there are many different variables to consider when optimizing the production of a diamond film a more efficient model has to be adopted to ensure time is not wasted on experiments that are essentially trial and error scenarios. A Taguchi optimization method was chosen due to its proven efficiency. Although it was never fully implemented within this research due to time constraints, all experiments conducted were designed with the aim of providing the ground work for the eventual running of the optimization method.

The Taguchi method has been used in many fields for optimizing several parameters on a single instrument, in a small number of experiments, in order to produce an ideal product as quickly as possible. This method is well documented in a wide variety of fields and its use in the Japanese industrial sector has been linked to its huge growth and success^[19]. This led to its widespread use for experiments in fields as varied as engineering^[20], chemical extraction^[21], advertising^[22], waste management^[24] and even economics^[23]. One of its most promising uses has been documented in several papers^[25-27] where the Taguchi method was used to optimize new CVD instruments. None of the Taguchi processes used the exact experimental set up that is being installed on the PDC PA-CVD here at the University of Bristol. This is why the use of the Taguchi method is still vital, all the past optimization processes all possess merits of their own to aid in the design and implementation of the optimization. Moreover it demonstrates that this method works for the optimization of CVD instruments, allowing greater confidence to be placed in the experimental design.

Experimental design

The Taguchi method follows a specific path when designing a new experiment, as laid out by R. Unal & E. Dean^[29] (**Figure 12**). This path allows for a reliable, efficient and, most importantly, non-biased experimental set up.

Quality Characteristics, Test Conditions and Noise Factors

The initial step ensures that target goals are obtained. When considering different industrial uses of diamonds, different qualities may be more important for different applications. Most of these have been looked at already but for the optimization of the new reactor, plus the creation of discrete ¹³C and ¹²C layers of diamond film, the most important characteristic to achieve is a small uniform grain size on the diamond film. This will show that

Presented at the 1991 Annual Conference
of the International Society of Parametric Analysts.

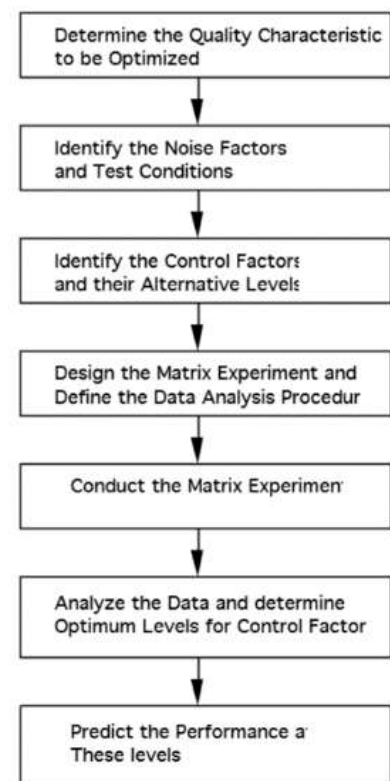


Figure 12. Taguchi method experimental design flow chart^[29].

a high quality film has been created and will limit the bleeding between isotopic layers through a well-defined boundary. These well-defined layers will be vitally important as any major discrepancies in the boundaries will blur the line between conducting and insulating layers, limiting their effectiveness and use. The diamond film quality will be quantified by measuring an average grain size for the surface diamond utilizing SEM imagine. Also the ratio of sp^3 to sp^2 carbons within the film, comparing the diamond, 1332 cm^{-1} , to graphite, D & G bands at $\sim 1450\text{ cm}^{-1}$, peak areas respectively from Raman spectroscopy.

The second aim proceeds from the fact that the production needs to be as reliable and quick as possible. Ensuring that the diamond film can be produced with a single script without fault is essential to ensure plenty of testable and workable material is created. Initial tests with the instrument have slowly increased its reliability with respect to both the plasma and the controlling software, enabling constant plasma production without fault for hours. Because of the deposition times all being the same length for initial optimization, the speed of deposition will be calculated by measuring the average thickness and dividing by the growth time to produce an overall growth rate in hours. While diamond quality cannot be sacrificed for growth rate, with two identically high quality diamond films, the faster growing film must be chosen.

Control Factors and their Alternative Levels

The different control factors have already been talked about in Chapter 2, so the exact parameters and outcomes will not be looked at in detail here. Instead a clarification of the choice of the alternative levels will be discussed. The decision for most of the parameters was settled upon from a combination of five main papers, utilized not only for their similar set up, but also their exemplar results and extended reporting of their synthesis methods. Most the values were chosen from an average spread of values from these papers^[2,7,6,49,50], combined with system limitations and improved scientific knowledge. For further use the papers will be referred to by their shortened names; ‘Suzuki’^[2], ‘Thick Film’^[7], ‘8-Inch’^[6], ‘Lux’^[49], and ‘Ultrananocrystalline’^[50]. The overall chosen parameters are shown in **Table 3**.

Table 3. The chosen Taguchi values for the optimization process.

Control Factor	CH ₄ concentration / % composition	Pressure / Torr	Deposition temperature / °C	Pulse frequency / kHz	Power / W (A) ^a .
Alternative Levels	1	100	800	50	3500 (~12)
	4	150	900	75	4500 (~15)
	7	200	1000	100	5500 (~18)
	10	250	1100	125	6500 (~21)

a. Current and voltage automatically set by the power supply, estimated value of produced amps in brackets

Methane concentrations will be run from 1-10% of the total concentration of gas in the reaction vessel.

Initial tests will be run in a hydrogen rich environment, which results in the rest of the gas mixture consisting purely of hydrogen, as this has shown to be the most effective at uniform diamond creation and provided the most stable plasma production. Ultrananocrystalline ran experiments with argon rich^{viii} environments and results showed 'large grains of a few tens of nanometers to 100 nm in size'^[50] were produced when using molybdenum deposition plates. This is thought to be due to collisions of excited argon molecules knocking off molybdenum from the cathode onto the substrate^[83] and resulting in uneven growth and nucleation along with the formation of C-Mo bonds. This can be halted through either using a heavier metal which has a mass more dissimilar to that of argon or removing argon from the deposition mixture. While the first solution could be achieved with tungsten, as it is both heavier and does not compromise on melting point range, as the reactor aims to be run at high temperatures. However, tungsten was not initially available and in more studies researchers used molybdenum over tungsten for comparison purposes. Therefore the much easier and cheaper use of hydrogen rich atmosphere was chosen. This makes even more sense when looking at the results from the above experiments, with the low ionizing energy of argon originally being an advantage for early system, but ultimately proving difficult to work with under the new high power system. Argon rich atmospheres also produces lower growth rates then with hydrogen rich atmospheres^[51], although this was seen in a MPACVD reactor so the results have to be looked at with caution. Hydrogen rich deposition reaction were also much more common in the literature, show by the all 5 papers utilizing DC PACVD^[6,7,49,50,2], only one had an argon rich experimental run, and even this included hydrogen rich deposition plasma as a parallel run.

After the decision to run hydrogen rich deposition mixture was made the values for methane concentration were chosen from the best runs of the different papers (**Table 6**) which allowed for a comparison of values. The lowest tested value of methane was from Lux and gave a value of 0.5%. But this showed no growth and the next tested value of 0.9% showed minor growth. Therefore 1% was chosen as the cutoff point used as a comparison point more than an expected high growth condition. Meanwhile 10% was chosen as the maximum methane concentration. While the highest value used, in 8-Inch, was 12%, and would be the best starting point for testing the limits of the instruments optimization, initial experiments showed ballas diamond formation at 5%, which is a sign for over saturation of methane in the system^[82]. In addition, the paper has no specific results to its run at 12% so the produced quality of diamond is not known. Therefore, sticking with a value more in the range of reported results will allow for a deeper understanding of the results in a more ideal concentration range. These concerns combined with the fact that none of the other researchers went near 12% for their optimized runs, the closest was 9% from the Thick Film paper, shows that it is probably not an ideal reaction condition. The middle values were chosen as an even spread, with one being right in the ideal

^{viii} Using argon as the main component of the deposition mixture (i.e. 90% Ar, 2% CH₄, 8% H₂).

zone of deposition, 4%, and the other being closer to the experiments of the remainder of the papers, 7%.

Pressure was chosen in a similar manner to methane concentration. The lowest run value was 100 Torr therefore this was chosen as the base line for the experimental runs as well. The baratron pressure gauges installed in the instrument, combined with the vacuum pump, have a 5 Torr error range so much lower pressures will result in too large an error range to be acceptable for testing. Little has been published on the effects of pressure on diamond quality in PDC PA-CVD systems. The most complete analysis the literature has is based on hot filament CVD systems, which show an increase in pressure results in an improvement in the diamond film^[52]. One paper ranges from 40 to 400 Torr, showing a shift from micro-crystalline diamond production to nanocrystalline diamond production above 200 Torr. But with none of the DC PA-CVD papers running experiments above 200 Torr there is no data for experiments at pressures that high. Because 200 Torr is the highest pressure used in all studies, this value was chosen here as well. It also came from some of the most favorable and seemingly reproducible experiments, those from the Lux paper. The other papers were all centered around 150 Torr, most likely due to them all being from the same research group, hence the choice for 150 Torr as an experimental condition as well. Then finally, to test the high pressure scenario; 250 Torr was chosen to see if high pressures were still able of producing nanocrystalline diamond in this PDC PA-CVD system.

Deposition temperature varied between the different papers. Because the range between all the papers was 550 °C there were evidently a lot of factors figuring into the optimum temperature for deposition. Aiming to cover this span of temperature was the intended starting point. Because the Taguchi range was chosen to reflect the spread amongst the papers, the values in **Table 3** were chosen. The highest value of 1100 °C was chosen to experiment on the effects of high temperature on the size of the diamond crystals. Because the instruments design allow for higher temperatures to be reached it is possible to experiment further, but limiting it to a known operational range from the literature and staying within an easy to reach level, thereby reducing the amount of modification required to attain the higher temperatures, will allow for a quicker optimization. The Lux paper stated that ‘successful deposition...was only possible within the cathode temperature range 900-1000 °C’, which needs to be considered for testing. This was the primary reason for the selection of both the 900 and the 1000 °C value. The final value was chosen as a lower end capping value. While deposition should occur at this temperature, and more importantly is easily readable by the pyrometer, it will not be ideal and probably will give a poorer result to compare against.

The pulse frequency proved more problematic in producing a range of values for testing due to the fact that only one paper, Lux, utilized a pulsed DC set up. A pulse/pause speed of 50 μs/50 μs (20 kHz), varied down to 75 μs/50 μs (~13 kHz), was used in these experiments. The instrument has the ability to produce pulses of up to 150 kHz, with pause durations up to 4.5 μs. These limits should be fully explored

considering the minimal testing that has been done in the literature into the pulse rates effects. By chance the default pulse rate is 100 kHz, and for simplicity, this was chosen as the pulse rate in all initial testing. The values were then chosen to spread around this, without reaching the maximum, to observe how the frequency varies the quality of the produced films. This resulted in the settled upon values of 50, 75, 100 and 125 kHz frequencies. Varying the pulse/pause ratio will be out of the scope for the initial Taguchi optimization due to the added complexity but may be explored in later testing.

The power initially was going to reflect the power levels used in the various papers. Unfortunately some of those powers were too large for the instrument to handle, with nanocrystalline reaching over 20 kW for example. While others did not have enough power being supplied to allow for deposition temperatures to be achieved, which occurred when attempting to recreate Lux conditions at 3.6 kW. In light of these results, and continuing improvements to the instruments limits (allowing for a greater operational power range^{ix}) produced the final power ranges. The lower value of 3.5 kW was chosen to reflect Lux's optimized run, with the new wire spacers finally allowing plate temperature to be achieved at this low power. The next two power levels were chosen as a spread across the experimental operating range already being used. 4.5 and 5.5 kW are either side of the most used power on this instrument. 4.75 kW was only chosen for testing as it was the highest power able to be put into the instrument without overheating the cooling system, but was not chosen to maintain an even spread of values. The highest power, at 6.5 kW, was then chosen to experiment with the effect of higher power and to observe the implications this would have on overall deposition. The higher power has been reported to produce higher quality diamond^[81,82] and therefore 6.5 kW should provide a high enough power setting to observe the differences relative to the lowest power setting of 3.5 kW.

Experimental Matrix and Data Analysis Procedure

To ensure all test conditions are covered and comparable results are produced at the end of the experiments a L16 orthogonal array^[72] was used to produce the experimental matrix (**Table 4**).

The L16 represents the number of factors, 5, and different levels that each of those factors can take, 4 with the 16 representing the number of experiments needed to be completed to fully optimize the system. An orthogonal array is a table of numbers where no two boxes on one row contain the same combination of numbers as any other pair of boxes in the same column. For example; experiment 1 has a pressure of 100 Torr and a pulse frequency of 50 kHz, no other experiment has those combinations of pressure and frequency. Also; experiment 10 has a deposition temperature of 1500 °C and a pulse frequency of 100 kHz, again with no other experiment having these same factors.^[29]

To ensure no bias towards the experimental results, the data analysis procedures have to be outlined and the optimum result agreed upon beforehand. All deposition plasmas will be analyzed using OES

^{ix} Some added after these experiments were concluded.

focused at the center of the plate and a few mm above the substrate. All spectra will be recorded as an average of 100 spectrum taken over 1 second, three times a deposition run; once at the beginning upon the addition of methane, once after 2.5 hours of run time, and the final spectrum will be taken 20 minutes before deposition is stopped. Experiments that produce analyzable material will be run through Raman Spectroscopy, taking three readings from each the edge of the disk, the center of the disk and along the radius, at three different radii. The ratios of sp^3/sp^2 will be calculated and averaged across all readings. All SEM images will be run on the edge, center and along three radii (equidistant between the center and edge). The size of the crystal structure formed will be characterized and, if possible, measured by averaging the crystal sizes of 10 crystals per SEM image.

Table 4. Fully constructed L16 orthogonal array produced for the Taguchi optimization experiments.

Experiment Number	CH ₄ Conc. / % composition	Pressure / Torr	Deposition temperature / °C	Pulse Frequency / kHz	Power / W ^a
1	1	100	800	50	3500
2	1	150	900	75	4500
3	1	200	1000	100	5500
4	1	250	1100	125	6500
5	4	100	900	100	6500
6	4	150	800	125	5500
7	4	200	1100	50	4500
8	4	250	1000	75	3500
9	7	100	1000	125	4500
10	7	150	1100	100	3500
11	7	200	800	75	6500
12	7	250	900	50	5500
13	10	100	1100	75	5500
14	10	150	1000	50	6500
15	10	200	900	125	3500
16	10	250	800	100	4500

a. Current and voltage automatically set by the power supply, estimated value of produced amps in brackets.

Run Experiment and Analyze the Data to Determine Optimum Control Levels

All experiments should be run with as little choice as possible on which experimental number to next follow. Using a random number generator for the selection will ensure no bias towards results or experiments are manifested. This will maximize results credibility and reduce errors in the final results. If possible, an automated script system will run all experiments without any knowledge of which

experiment was run until after completion and analysis, although this may be difficult to achieve with little benefit.

After all experiments have been run the produced films are to be analyzed using Raman Spectroscopy and SEM imaging as noted before. The quality will be ranked and placed on graphical arrays for comparison. Further to this the variation in quality level will be averaged and the spread calculated to allow the selection of ideal results. From all experiments, the size of the average diamond grain θ_a grown under all experiments running a single Control Factor Level (e.g. 100 Torr) will be compared to the average grain size from every experiment, θ_{avg} . This will produce a 'score' based on one Control Factor alone. An ideal θ score will be as low as possible, reflecting the smallest crystal size produced. However, to produce a comparable score to the others θ must be altered. To do this a percentage difference to the average score is calculated and the negative of the produced value is taken. Then the sp^3/sp^2 ratio χ_a produced from all experiments running a single Control Factor Level will be calculated and compared to the average across every experiment, χ_{avg} . Again the percentage difference will be taken but remained unchanged as the highest score will result in the highest ratio of diamond relative to graphite in the sample. Finally the range in crystal sizes σ_a from each experiment running a single Control Factor Level will be summed, and a percentage difference to the average across all experiments, σ_{avg} , will be calculated. An ideal score for this Quality Characteristic will be the lowest value possible, so again the negative of the produced value will need to be taken.

These values will then be combined with each other to produce the highest 'score' of values per Control Factor Level, ϕ . By doing so the Control Factor that produced the best results can be observed. For example^x; if all 100 Torr experiments produced a ϕ value of 20, 150 Torr a value of 15, 200 Torr a value of 17, and 250 Torr a value of 19, then the ideal deposition conditions will be at 100 Torr.

To calculate a ϕ for a specific grouping of Control Factor Levels^{xi}, a simple summation of each levels ϕ relative to the ϕ_{avg} will produce a score for the hypothetical set up. This allows for an ideal set up to be found, even if it had not been run in the initial experimental matrix.

Predict Performance at Optimum Levels

After calculating ϕ for all possible theoretical and tested combinations of Control Factors, the highest scoring experimental set up will reflect the ideal experimental conditions. If this set up has not already been conducted then one further deposition run should be done to ensure that this in fact produces an ideal diamond film relative to all others done before hand.

^x Using false numbers with no bases on actual experiments, just used for representational purposes.

^{xi} e.g. 100 Torr, 4% methane, 1100 °C, 50 kHz pulse frequency, and 6.5 kW.

Post Optimization

After completing the optimization of the new PDC PA-CVD system by the Taguchi Optimization method, reliable films of diamond should be quick and easy to manufacture. But further work will always be necessary. This optimization sets several variables to constants throughout all experiments, such as gas flow rate, argon concentration, plate separation distance etc., and therefore while the system will be producing high quality diamond further Taguchi optimizations could be done to not only further improve the produced diamond film quality but also to learn how variables affect the overall system, especially for those less documented in the literature.

While the current experimental set up outlined above is aimed at producing a working and reliable instrument quickly, more time could be put into producing an optimization for all variables in the system. This would require minimal extra calculations effort and only a small increase in the number of experiments run. Overall this could provide a huge amount of data on how the new PDC PA-CVD instrument operates and would allow the exploration of many further research paths, especially isotopic film formation, as quickly as possible upon the steady stream of high quality diamond films to be produced.

Project Plan

Before the Taguchi optimization process could be implemented the instrument must first be able to conduct rudimentary depositions of diamond films. While high quality was not a necessity, just proof of concept for the instrument, the aim should be to allow for not only making the calibration more specific towards the eventual Taguchi optimization, but also to allow for amendments to be easily implemented to the Taguchi method for an improved final result. Initial tests focused on plasma functionality and stability to allow for an ideal basic environment for deposition to commence within. Then further tests were conducted with deposition conditions; initially replicating promising literature results then modifying them according to the instruments demands. The experiments conducted are outlined below.

Experimental Conditions

Several non-deposition runs were conducted prior to initial deposition for various plasma analysis and instrument testing. While all of these are not individually listed here, results collected from these experiments have been noted and experimental conditions listed with the results.

Hydrogen and argon gas of 99.999% purity for both was purchased from Air Liquide^[84]. Methane of 99.995% purity was purchased from BOC^[85]. No further modification to the gasses was done prior to introduction into the deposition chamber.

All operational systems were controlled through an in-house written Delphi program, allowing control of the pressure, power, gas flow rates and composition. While it was constructed to follow an

operational script, this was never tested due to consistent, high quality deposition never fully being realized. Scripts (**Figure 13**) will allow for easy automation of the manufacturing process upon completion of optimization.

Deposition experiment 1 was set up with 0.5 mm tantalum wire spacer on both the upper and lower molybdenum plates, with the lower plate also utilizing the copper ‘C’ spacer. The deposition chamber was vacuumed down to ~35 mTorr and then raised to 15 Torr in hydrogen (400 sccm). The plasma was struck with 350 W (100 kHz pulse frequency). The pressure and power were raised to 87 ± 14 Torr and 4.75 kW (12.84 ± 0.5 A) respectively and maintained at these settings until the substrate began to glow and a stable temperature of 745 ± 18 °C was achieved, and maintained, for ~3 minutes. Methane was then added to the chamber at 12 sccm (3% total volume, 412 sccm

total gas flow) and a 1 hour deposition commenced onto the non-polished molybdenum deposition plate with 1cm² identically seeded (18-36 nm nanodiamond seed size) molybdenum and p-type silicon plates placed on top. After deposition was completed the methane gas flow was stopped and the plasma maintained for another 5 minutes in pure hydrogen before the chamber was vacuumed down to ~40 mTorr and then brought up to atmosphere in argon. The plasma during the experiment was monitored with Optical Emissions Spectroscopy (OES), and the substrates were analyzed with both Scanning Electron Microscopy (SEM) and Raman Spectroscopy. Further discussion of this experiment will be referred to as Ex1, with the results listed as Mo1, SMO1, and SS11 for the molybdenum plate, the seeded molybdenum substrate and the seeded silicon substrate respectively.

Deposition experiment 2 was set up with 0.5 mm tantalum wire spacer behind the cathode molybdenum plate, with the lower substrate set up with a 0.75 mm tungsten wire on top of the copper ‘C’ spacer. The deposition chamber was vacuumed down to ~35 mTorr and then raised to 15 Torr in hydrogen (500 sccm). The plasma was then struck with 350 W (100 kHz pulse frequency). The pressure and power were then raised to 95 ± 6 Torr and 4.75 kW (12.84 ± 0.5 A) respectively and maintained at these settings until the substrate glowed and a stable substrate temperature of 815 ± 15 °C was achieved, and maintained, for ~10 minutes. Methane was then added to the chamber at 20 sccm (4% total volume, 520 sccm total gas flow rate) and a 1 hour deposition commenced onto the non-polished molybdenum deposition plate used in the last experiment. A 1 cm² identically seeded (18-35 nm nanodiamond seed

```

Lux 4% CH4.txt - Notepad
File Edit Format View Help
SystemReset
0.0, PSU OFF, VC

AlertCathodeTemperature = 1100
AlertAnodeTemperature = 1100

PPSUStrikeVoltage = 400 V

VGVMode = Pressure
VGVSetPoint = 1 Torr ;why Set

PPSURegMode = Current
PPSUCurrent = 0.5 A
PPSUPulseFrequency = 20 kHz ;just se

ValveHydrogen = ON
MFCHydrogenSetPoint = 300 sccm

PPSUStrikePlasma
Time = 240 s

VGVMode = Pressure ;needs t
VGVSetPoint = 200 Torr
PPSURegMode = Current ;should
PPSUCurrent = 4.4 A
PPSUVoltage = 800 V

```

Figure 13. A section of the PDC PA-CVD instrument script for deposition. Deposition conditions were based off Lux *et al.*'s work^[49].

size) molybdenum and p-type silicon plates were placed on top and a small droplet of seeding suspension was placed directly onto the molybdenum deposition plate. After deposition the plasma power was reduced to 1 kW over ~30 seconds before being completely turned off and the chamber immediately vacuumed down to ~40 mTorr. The chamber was then brought up to atmosphere in argon. The plasma during the experiment was monitored with OES, and the substrates analyzed with both an optical microscope and Raman spectroscopy. Further discussion of this experiment will be referred to as Ex2, with the results listed as Mo2, SMO2, SSi2, and SS2 for the molybdenum plate, the seeded molybdenum plate, the seeded silicon plate and the seeding substrate respectively.

Deposition experiment 3 was set up identically to Ex2. The deposition chamber was vacuumed down to ~25 mTorr then raised to 15 Torr in hydrogen (500 sccm). The plasma was struck with 350 W (100 kHz pulse frequency). The pressure and power were raised to 95 ± 6 Torr and 4.75 kW (12.84 ± 0.5 A) and maintained at these settings until the substrate glowed and a stable temperature of 815 ± 15 °C was achieved, and maintained, for ~2 minutes. Methane was then added to the chamber at flow rates between 0 and 50 sccm (0-10% total volume, 500 sccm hydrogen gas flow rate maintained) over ~35 minutes. The flow rate was then set at 25 sccm (5% total volume, 525 sccm total gas flow rate) and a 2 hour deposition commenced onto the non-polished molybdenum deposition plate used in the previous experiments with a strip of non-seeded n-type silicon placed along the radius on the molybdenum plate (~5 cm long and no wider than 1 cm). After deposition the plasma power was turned off and the chamber vacuumed down to ~40 mTorr before argon was introduced to raise the pressure to atmospheric. The plasma during the experiment was monitored with OES, and the substrates analyzed with SEM afterwards. Further discussion of this experiment will be referred to as Ex3, with the results listed as Mo3, and NSSi3 for the molybdenum plate and the non-seeded silicon strip respectively.

Deposition experiment 4 was set up with 0.75 mm tungsten wire placed behind the cathode and 1 mm tungsten wire on top of the 'C' underneath the substrate. The chamber was vacuumed down to ~30 mTorr then raised to 15 Torr in hydrogen (500 sccm). The plasma was struck with 400 W (100 kHz pulse frequency). The pressure and power were then raised to 95 ± 6 Torr and 4.75 kW (12.84 ± 0.5 A) and maintained at these levels until both the cathode and substrate glowed and a suitable substrate temperature of 850 ± 15 °C was achieved (using the same pyrometer as Ex2, cathode temperature not measured), and maintained, for about ~2 minutes. Methane was then added at 20 sccm (4% total gas volume, 520 sccm total gas flow rate) and a 30 minute deposition commenced onto the same molybdenum substrate with a 1cm^2 pre-seeded (18-35 nm nanodiamond seed size) molybdenum substrate. After deposition the power was removed and the chamber vacuumed down to ~40 mTorr before argon introduction to raise the internals to atmospheric conditions. The substrates were analyzed with Raman spectroscopy and SEM. Further discussion of this experiment will be referred to as Ex4, with the results listed as Mo4, SMO4 for the molybdenum plate and the seeded molybdenum substrate respectively.

Table 5. Deposition conditions for conducted experiments.

Experiment number	CH ₄ conc.	Total Gas Flow Rate / sccm	Power (Amps) / kW (V)	Pressure / Torr	Deposition Time / minutes	Plate Temperature / °C
1	3%	412	4.75 (12.84±0.5)	87±14	60	745±18
2	4%	520	4.75 (12.84±0.5)	95±6	60	815±15
3	5%	525	4.75 (12.84±0.5)	95±6	120	815±15
4	4%	520	4.75 (12.84±0.5)	95±6	30	850±15

Issues and Modifications

A significant number of issues arose during construction and initial testing, and these delayed the instrument start up and prevented experimental running within the project time limits. Many modifications were eventually implemented to the initial design to allow for the creation of suitable deposition conditions, without damage to the instrument, within the chamber.

Feedthrough Issues

The power for the PDC PA-CVD system was directed into the chamber through the cathodes via two copper water cooling pipes, and directed out through the grounded substrates via copper water cooling pipes. These components were bought as stock components and installed into the system through a sunken entrance hole (highlighted in yellow on **Figure 14, a**) with a copper gasket. The feedthroughs were separated from the grounded gasket complex through the use of a ceramic insulator. Due to the design of the part, and the sunken entry point where the feedthroughs were introduced into the chamber, the entire system, when lowered to strike pressure, created a potential difference requiring a lower strike voltage than between the deposition plates. This not only stopped useful plasma creation but also short circuited the system.

Initially TorrSeal^[73] was piped into the recess. The low pressure applications of TorrSeal were considered to be appropriate to the system.



Figure 14. The feed through in working order after final modifications were completed. The small feed through opening (a), highlighted in yellow, was leading to the issues with arcing, while the glass rods (b) and the flexible coolant pipes (c) were installed to counter this issue.

Unfortunately after two runs the system continued to arc without any obvious cause seen through the viewing window. Upon the removal of the feed through component for the cathode, it was discovered that the TorrSeal had broken down under the high voltages used for striking the plasma. Further tests (placing unset TorrSeal under low pressure) showed that the TorrSeal contained air pockets within it, leading to small air paths for the system to arc through. This resulted in carbonization and eventual deposition of carbonized material, and a permanent circuit for the electrical flow.

The TorrSeal was removed and two glass rods were placed around the copper feedthroughs (**Figure 14, b**) and onto the factory spec ceramic protectors described above. Then TorrSeal was again added and cured at a higher temperature (~80 °C) to aid in air removal from the system. Flexible coolant pipes were also installed on both the bottom (**Figure 14, c**) and top plates (**Figure 15, b & c**) and the cathode and substrate were brought closer together in an attempt to favor current flow between the plates and lower the required strike voltage. The distance was reduced from ~25 mm (**Figure 15, a**) to ~6 mm (**Figure 10, D**). After reinstallation voltage tests were conducted and a similar failure was observed. Voltage again created a short circuit across the TorrSeal, passing under the installed glass, but only through one of the two cathode feedthroughs this time. This single feedthrough was replaced with a silicone based sealant with a higher breakdown voltage, assembled in a similar manner, and reinstalled. This set up has proved worthwhile (with the other TorrSeal sealed feed through having a near perfect glass to ceramic contact, therefore eliminating the voltage pass through) and no further issues occurred. The only noted change was the silicone sealant changing from a clear to a milky color after several runs, but no alteration in the systems resistance was noted after more than 20 full power runs.



Figure 15. The initial deposition plates set up with the large electrode gap and inflexible water cooling pipers (left), and the final set up with the shorter interelectrode gap (not shown) and the new flexible piping for plate movement (right).

Substrate and Cathode Temperature Control

Once the feedthrough issues were corrected, the reactor could be brought up to deposition conditions to commence initial tests. Unfortunately during the first high power runs of ~1.5 kW the stainless steel clips being used to support the top plates (both the copper spacer and molybdenum cathode) expanded

in the heat generated, producing a gap between the plates and the water cooling system. While this initially allowed for deposition temperature to be achieved in the cathode, as the power was raised a secondary plasma formed between the plates and the cooling block, leading to eventual arcing and shutdown of the system. Extra clips were added (from the initial 3 to ~10) and those added were placed in a vice to decrease their span and therefore hold the plates firmer. This proved to work in holding the plate up until ~3.5 kW where a slight separation started to be visible again.

At this power level further complications arose. As the power increased a bumping in both the substrate and cathode cooling plates could be heard. This was thought to be the copper spacers being too effective at thermal energy removal and therefore not allowing the molybdenum plates to reach deposition temperatures while raising the temperature of the water above boiling while it circulated. Initially to combat this copper 'C's were cut to reduce the thermal contact area and provide a low pressure air barrier to slow thermal diffusion. Due to a restraint in material resources on hand only the substrate had a 'C' produced and due to time constraints further tests proceeded while it was being manufactured.

Tantalum wire (0.25 and 0.5 mm) was used to aid in the spacing of the plates while the 'C' was being produced. While the 0.25 mm wire proved too small for effective thermal insulation of the molybdenum the 0.5 mm wire allowed the substrate to reach optimum operating temperature and eliminated the bumping in both plates cooling lines up to 4.75 kW power input. It was discovered that the added bulk of the wires enabled the clips to hold the cathode plates much tighter and even at high powers no separation was observed. A reduction in the reactor casing water cooling flow rate, thereby increasing the plates flow rates along the parallel system, enabled powers to be



Figure 16. The different cooling systems utilized on the PDC PA-CVD reactor. From left to right; the full 3 mm thick copper spacer with thermocouple slot cut out, the 1 mm thick copper 'C', the 0.5 mm thick tantalum wire, and the molybdenum deposition plate.

raised to 5 kW before bumping was heard. Again, due to time constraints, initial deposition runs were conducted on this system (including the 'C' installed after its arrival). Tungsten 0.75 mm and 1 mm wire were tested upon arrival and final deposition runs incorporated the 0.75 mm W wire on the cathode with the 1 mm W wire on the substrate allowing for a glow and optimum temperatures on both plates. To aid in monitoring the water temperature thermocouples were placed along the existing water cooling pipes to monitor the temperature change. This allowed for more warning concerning the rise in temperature of the system when venturing to higher powers.

Plasma Stability

Argon, as explained in Chapter 2 above, was chosen as a test gas due to its low energy of ionization. Its inertness increased safety during initial tests. This meant that low pressure tests were more likely to work with minimal strain on the system. However, the produced plasma was very diffuse and inherently unstable. The low pressure tests required power supplies too small for the machine to handle and due to the rise in voltage needed to create a plasma at higher pressure this put the feedthrough system under risk. The power supply, chosen for this reason but not ideal for the weakened system, can produce a high voltage burst to aid in plasma striking. This was forcing too much power through the system and leading to easy arcing formation and improper striking locations of the plasma system (such as between the cathode cooling pipes and the reactor wall). Initially, increasing the pressure was believed to reduce arcing within the system but at higher pressures, and higher power to maintain the plasma evenly across the substrate, the diffuse argon atmosphere led to frequent arcs. This put the power supply into automatic shutdown mode to protect itself and resulted in a system reset. After several tests aimed at increasing plasma stability, and in an attempt to create sufficient heat on the substrate, a pure hydrogen plasma was tested at low pressure (~1 Torr) with the aim to incorporate more temperature into the plates. The plasma stability was greatly increased, and the power supply was striking much more reliably above its threshold range. Further tests with increasing strike powers and pressures showed that the feedthrough modifications worked and plasma stability was much improved with the hydrogen system, resulting in the use of the argon purely to open up the atmosphere.

While stabilizing the high power plasma throughout these experiments, two unexpected events occurred. Firstly, the diffuse argon plasma tended to arc and shut down the power supply (forcing it into a safety mode). The arcs originated from a stainless steel clip supporting the cathode plates, resulting in a vaporization of these clips (fortunately this did not cause a critical failure of the support system). Secondly, the plasma arced from the cathode to the thermocouple monitoring the substrate temperature resulting in a broken thermocouple. This not only removed the ability to directly measure the substrate temperature through the computer software, but also highlighted a flaw in the design: a point of increased field strength leading to an increase in arcing behavior from the thermocouple itself. A further concern was the deposition of copper over the cathode and substrate during a low pressure extended run. This was due to copper being more similar in mass to argon, relative to atomic hydrogen, and, as a result, kinetic energy between the argon and copper was easily exchanged and sputtering of copper from the spacing disks to both the molybdenum plates and the instrument supports occurred. To enable further testing the copper was removed using concentrated nitric acid however this resulted in the electrode having a lower quality finish than before (although no major finish was incorporated beforehand). Pitting was also seen, similar to that noticed by *H. Lee et. al.*^[50]. These both resulted in a heavily damaged cathode and substrate, reducing their effectiveness for full scale deposition experiments.

Chapter 5: Experimental Results and Discussion

Limited running has produced limited results but valuable information has been gained from the instrument to aid in exploring the capability of this instrument to produce diamond. These can then be further applied to the Taguchi method to allow for refinements of the optimization parameters, increasing its effectiveness.

Initial Plasma Tests

Before deposition runs commenced the plasma was analyzed using Optical Emissions Spectroscopy (OES). This allowed us to better understand the instruments' capabilities and behavior. Several runs were conducted, varying the power or the pressure of the system, to observe how the plasma reacted.

First runs involved varying the power output while maintaining the same pressure and gas flow rate (**Figure 17**). With the limited control of the substrate and cathode temperatures under the current configuration, combined with a lower temperature limit of ~ 700 °C on the LandMark X pyrometer, the temperature levels varied with the power but could not be recorded. Therefore the temperatures were treated as proportional to the power input for the purpose of this experiment.

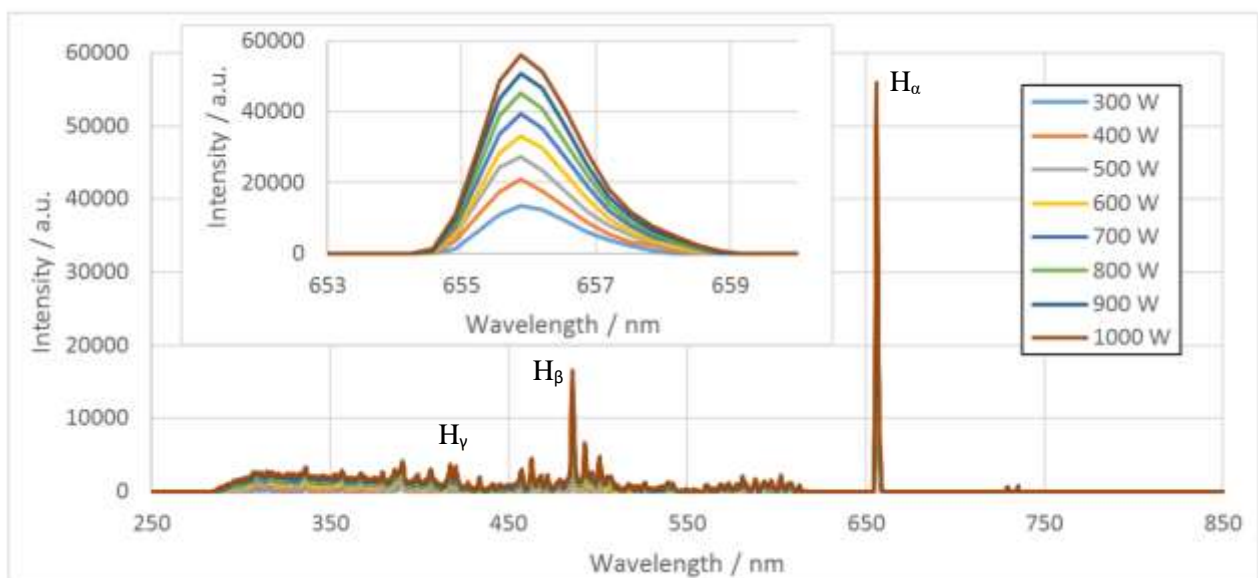


Figure 17. OES spectrum showing the effects of varying power on a pure hydrogen plasma (14 ± 3 Torr, 100 kHz, 400 sccm H_2). The H_{α}^{10j} line, at 656 nm, is expanded in the smaller graph.

Clear production of the hydrogen Balmer series, with H_{α} at 656 nm, H_{β} at 486 nm and even a small indication of H_{γ} at 434 nm can be immediately seen. These spectra were conducted over an hour, with a software malfunction half way through (requiring a system reset), and yet the spectra all appear identical apart from the variations in intensity. This indicates a stable system and suggests extended diamond fabrication runs will prove successful.

This inherent stability is noticed when looking at the change in intensity as the power increases. The smaller graph within **Figure 17** shows this with reference to the H_{α} line. Steps of 100 W were used

across the experiment (ensuring that the entire substrate was covered with plasma at all powers) and a remarkably linear step growth of intensity is seen. Such predictable plasma behavior is not possible to achieve on a second by second basis, as seen here, on other CVD reactors.

Second experiments were conducted by varying the pressure while maintaining the same power output. As **Figure 18** shows, a similar trend of linear variation is also noticed in this pressure experiment.

Both of these experiments shows simple behavioral characteristics of the PDC PA-CVD plasma. While they provide only a minimal insight to the deposition process, this has allowed for a greater understanding about producing optimum depositions conditions and the limit of the instrument. The plasma can only operate within a window of pressure and power without either partial substrate coverage, occurring at too low power or too high pressure, or too diffuse plasma with indirect heating and consistent arcing, occurring at too high power or too low pressure. While this ‘Goldilocks’ zone (**Figure 19**) was greatly increased with the use of the hydrogen feed gas over argon, it is still necessary to observe the plasma during operation, especially during earlier experiments, to prevent high voltage faults from occurring and possibly damaging the system. The zone increases in size as the power and pressure increase. This is aided by a smaller percentage power

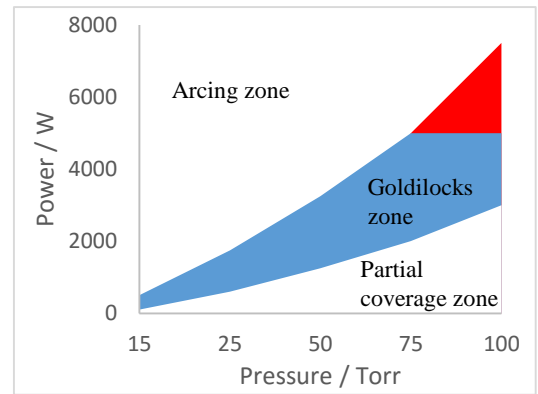


Figure 18. Visual description of the power/pressure ‘Goldilocks’ zone. Values above 5 kW are extrapolated points.

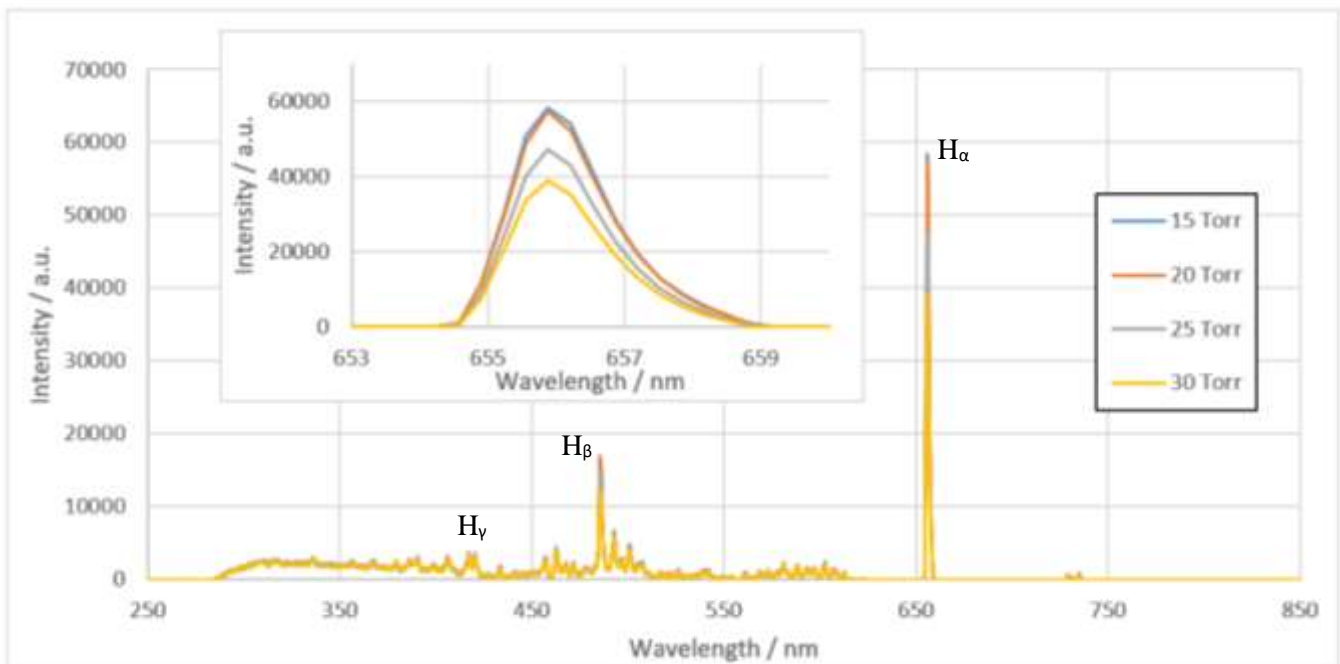


Figure 19. OES spectra showing the effects of varying pressure on a pure hydrogen plasma (1 kW, 100 kHz, 400 sccm H₂). The H_α¹⁰ line, at 656 nm, is expanded in the smaller graph.

increase at higher output levels, as each increase increment^{xii} remains the same. The pressure variation around the set point requires caution to be taken ensuring that uneven deposition or arcing does not occur at either high or low pressure. Because the computer controlled system cycles the pressure by up to 30 Torr at high pressure, this had to be closely monitored while improvements to the system were being made.

With the pressure cycle range reduced to acceptable levels these experiments allow for an optimum range of pressure to be exploited for Taguchi optimization. The discovery of the ‘Goldilocks zone’ for pressure and power produced combinations to be avoided upon optimization, as they will result in either improper deposition or uneven deposition and arcing. While the initial chosen taguchi values appear to fall within this zone, observations of the deposition plasma upon starting an experiment with parameters falling within these extremes (i.e. high power and low pressure) is necessary to ensure that successful deposition is possible.

Ex1

The first deposition run was conducted with the aim of replicating the conditions that *Lux et al.*^[49] laid out on their most successful deposition, allowing alterations only to accommodate the limits of the system. While most conditions were met from **Table 6** several had to be altered. The cathode temperature could not be attained within the instrumental set up and the substrate temperature could only be reached through an increased input of power^{xiii}. Also the required pressure could not be reached. This was because the

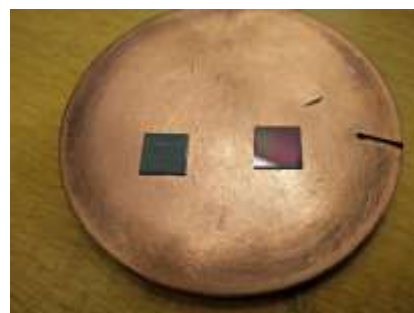


Figure 20. Produced films on SMo1 (left) and SSi1 (right) from Ex1.

voltages needed to produce a stable plasma with full substrate coverage at such pressures were above the limits of this instrument. This was partially offset through an increase in the gas flow rate. Most other conditions were attained and the experimental procedure was followed as closely as possible.

OES monitoring of the deposition plasma immediately showed issues with the system. As seen in **Figure 21**, the hydrogen Balmer series is evident with the peaks at 656 and 486 nm, giving relative values to the other peaks when comparing to a pure hydrogen plasma. Unfortunately a sharp peak at 388 nm is also seen which corresponds to the vibration band of CN B-X emission^[76]. The presence of these peaks indicates a leak in the system and therefore suggests that impurities are being introduced into the system. Other molecules, such as O₂ and Ar^{xiv} will also be introduced along with the nitrogen. The low concentrations will mask their produced spectra but will have varying effects on the produced diamond, and will, most likely, result in lowering the quality.

^{xii} 10 W minimum per step power increase.

^{xiii} 4.75 kW from 3.6 kW.

^{xiv} Being the next most common atmospheric gasses.

The main issue with the nitrogen leak is its effects on the main diamond growth species, C_2 and CH ^[13,14]. The CN radical is formed due to the stability of the $C-N$ triple bond, and once formed is unreactive and removes a molecule of carbon from any deposition involving reactions. This, combined with the reaction route being preferential in energy terms, quickly removes any carbon species that otherwise would produce the C_2 or CH radicals, severely limiting the growth rate. The small size of the peaks at both 431 and 516 nm, corresponding to CH and C_2 respectively, show how severely limited the growth had become due to the nitrogen leakage. Nitrogen is also linked directly with a decline in diamond quality^[11,61], through the increased growth of sp^2 amorphous graphite instead of diamond, which supported the prediction of poor growth results until the leak could be fixed.

Once removed from the instrument, obvious signs of growth could be seen, with the silicon substrate, (SSi1), gaining a birefringent quality, while still retaining its polished shine, and the molybdenum substrate, (SMo1), becoming dark matt in color (**Figure 20**). The films were inspected using Raman spectroscopy. While the molybdenum deposition plate showed no signs of growth, the seeded silicon (SSi1) and molybdenum (SMo1) substrates showed a visual change of both color and surface texture and therefore were examined. As **Figure 22** shows, both plates produced definite growth, but unfortunately were limited mostly to amorphous graphitic growth, with a double humped peak around $\sim 1450\text{ cm}^{-1}$, being characteristic of the D and G bands of graphite^[78], and a second peak at $\sim 750\text{ cm}^{-1}$ both being key characteristics for the presence of nanocrystalline and amorphous carbon^[77]. This could point towards nanocrystalline diamond growth if the nitrogen leak was not present, further supported by a peak present in both spectra at $\sim 1140\text{ cm}^{-1}$. This peak has long been taken as proof of production of nanocrystalline diamond. However, recently this has been shown to be dangling trans-polyethylene chains on the surface of diamond^[79]. Due to nanocrystalline diamond possessing a much greater surface

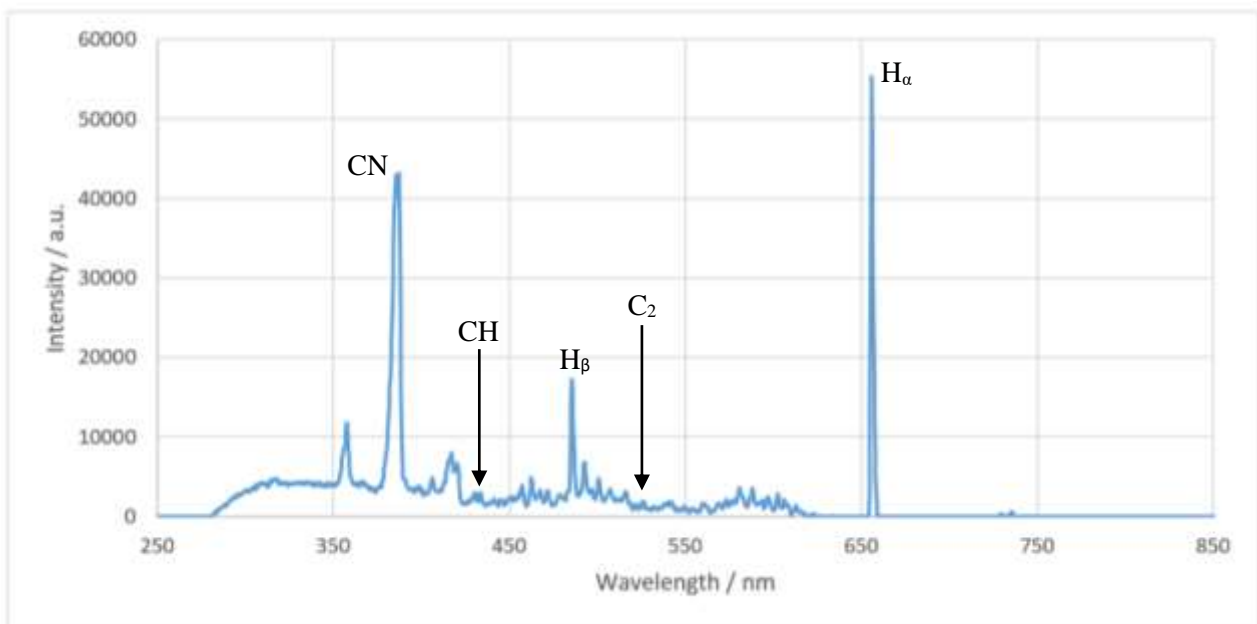


Figure 21. OES spectra of Ex1 during deposition.

area than microcrystalline, and especially single crystal diamond, the number of these dangling carbons greatly increases relative to the volume of diamond. As a result, the peak is more evident in nanocrystalline diamond than in any other kind. Unfortunately due to the lack of a peak or shoulder representing the 1132 cm^{-1} diamond peak off the main graphite peak the quantity of any produced diamond will be small and practically irrelevant when looked at completely. SEM was also conducted on the samples in an effort to see whether any regular growth was evident, or if possible diamond-like growths could be seen.

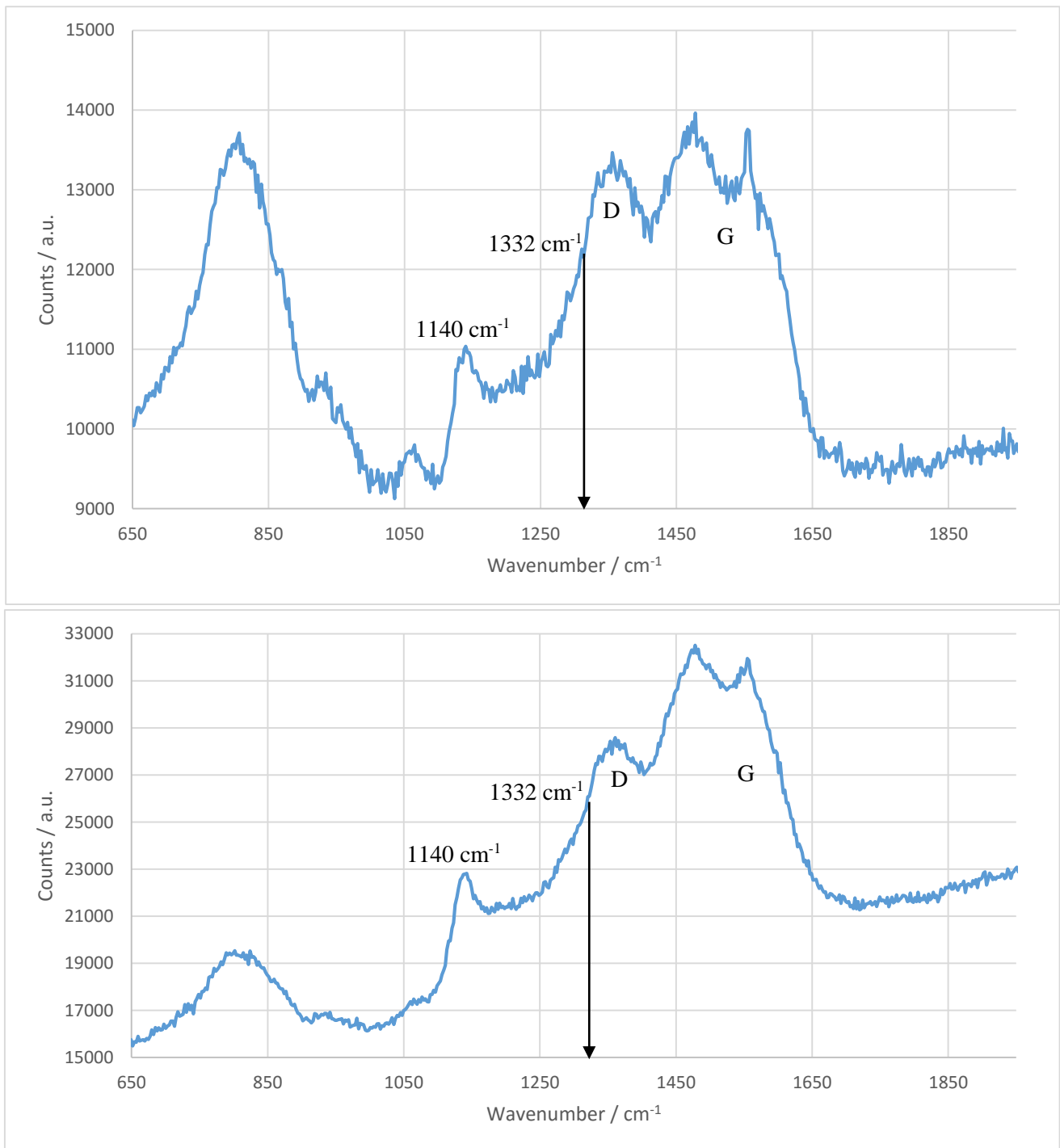


Figure 22. Raman Spectrum of SSi1, top, and SMo1, bottom (514 nm excitation wavelength, 10 second exposure, 180 spectra average).

What is immediately evident on the SEM images is the variation in growth size between the molybdenum and the silicon substrate (**Figure 24**). Growth has definitely occurred as the seed size is much smaller than the size of the current growths. The smaller silicon deposits are still roughly twice the size of the initial seeding particles^{xv}, with greatly increased density on the substrate. While both images were taken at the same magnification, the molybdenum growth appears significantly larger than the silicon. The growths are a few microns in diameter, but are also much less uniformly deposited than the silicon, and they also appear in lower

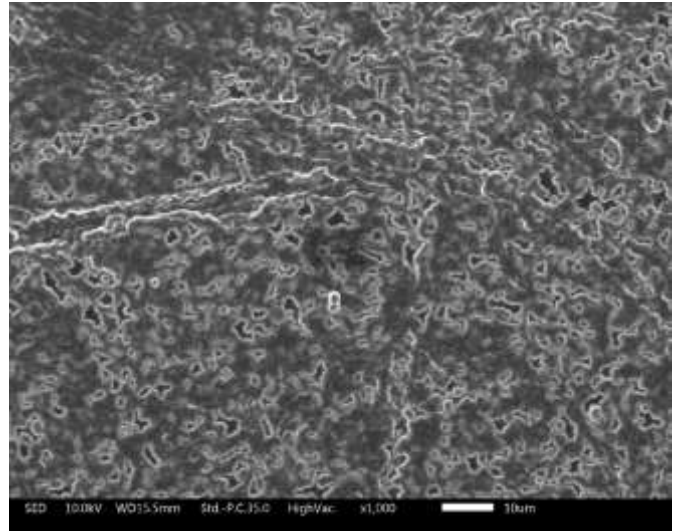


Figure 23. SEM image of SMO1, highlighting the non-uniformity of the created deposition.

density. This is more clearly noticeable in **Figure 23**, where many deposition pockets and holes can be seen. It is most likely that some nucleation has occurred on the molybdenum, and most of the growth was on existing seeds. As the seeds are mainly located in defects on the substrate surface, and the growth mainly occurred along defect paths, it explains why the layer of growth is uneven on the molybdenum substrate.

The silicon substrate showed a much more even growth but this was countered with a much smaller crystal size. The density of grown crystals on the substrate, as mentioned before, is much higher than the seeding material. This shows that not only has growth occurred on the nanodiamond seeds, but nucleation has also occurred at a substantial rate directly onto the substrate. The majority of the material

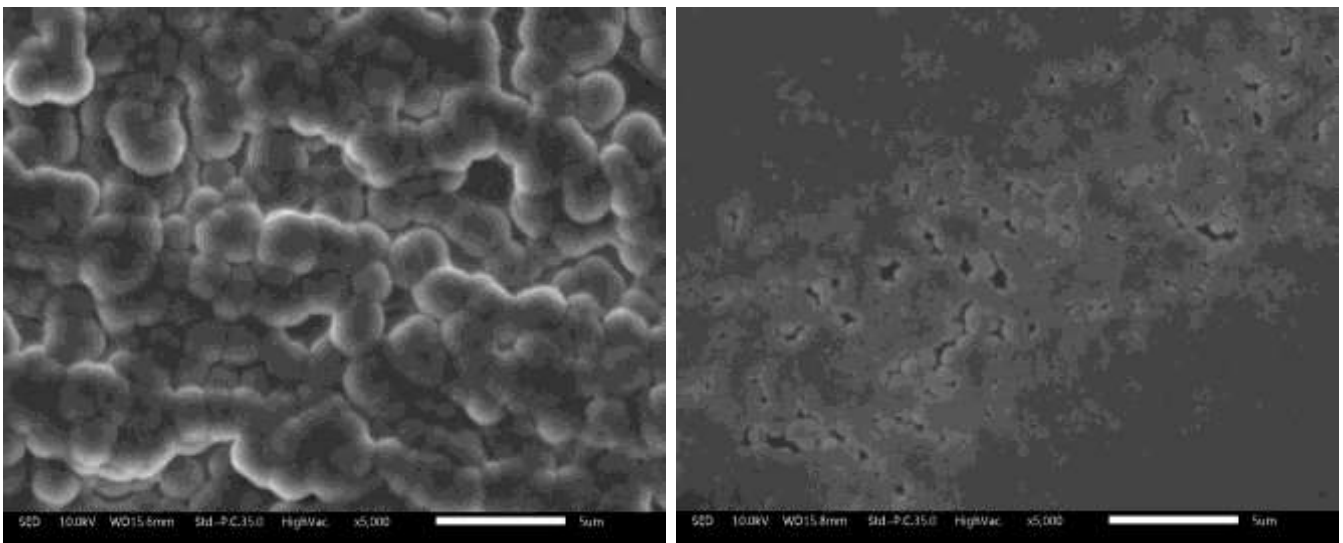


Figure 24. SEM images of SMO1 (left) and SSi1 (right). Both are taken at 5k magnification and show the variation in growth size between each other.

^{xv} 16-32 nm original seed size.

was covered in uniform growth which produced featureless poorly focused SEM images, forcing pictures of defects to be the main focus. Overall only a very small percentage of coverage was low seeding density as seen in **Figure 24, (right)**. These low density features appeared to be formed during the seeding process leaving streaks of low density seeded sections, due to the nanodiamond suspensions streaking off the substrate during drying. This could also be due to minor substrate defects from accidental physical damage.

Overall the growth rate and nucleation density appear promising but the shape of the particles themselves do not reflect quality diamond and will need to be investigated further. While ideal growth will produce rectangular shapes, these SEM images clearly show spherical growth. This is not only due to an incorrect concentration of methane in the system, and the result of graphite production, but is also linked to oxygen in the system^[64]. The spherical growths could be linked with ballas diamond growth but due to the lack of a scaly surface to them, and looking at *Bühlmann et al.*'s paper^[81] it is suggested that they more closely resemble graphitic deposits, As there are several similarities, especially when comparing with the Raman spectrum, closer images would produce a more definitive understanding. These growths could also occur due to nitrogen addition and may be linked to the air leak seen in the system^[60].

In following the *Lux et al.* script, a 5 minute plasma containing hydrogen only commenced after a deposition run of one hour. While this may have aided in cleaning the surface for large depositions, it was thought to have caused some of the features present in these results. Further experiments were conducted without this final step, and active measures were taken to limit the produced films exposure to the strong etching and removal capabilities of a pure hydrogen plasma system after the long deposition cycle. This combined with the new components brought in for the second experiment allowed improved deposition conditions to be run with the aim of producing improved films.

It has been shown that films can be deposited under the above conditions, meaning not only that the new PDC PA-CVD instrument works, but also that the parameters used here are not too far from high quality depositions conditions. Therefore the Taguchi values used in the eventual optimization should be chosen to be around these values. This is already the case due to basing both the Taguchi values, and the parameters for this experiment, off the *Lux et al.*^[49] paper, but gives confidence to the new instruments correlation with the literature, and the results that have been produced.

Ex2

After reviewing the results from Ex1, the second deposition run was set to address the issues in the first experiment. The main aim was to achieve higher temperatures, for aiding in sp^3 vs sp^2

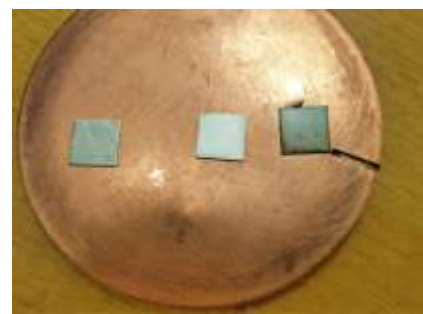


Figure 25. Produced films from Ex2. Non-deposited on seeded molybdenum substrate, SMO₂, and SSi₂ (from left to right).

deposition, and to move away from the literate deposition and to produce a procedure more tuned for this instrument.

The set up changes were designed to aid in reaching higher temperatures on the substrate and cathode. Thicker wire spacers on the substrate^{xvi} and cathode^{xvii} allowed the substrate temperature to reach up to 850 °C, but with the pyrometer cut-off limit the cathode temperature was not high enough to be measured, before bumping was observed, again in the cathode cooling pipes. This allowed for nearly a 100 °C increase for deposition. Further to this, the plasma was brought up to deposition conditions as quickly as possible in order to reduce the amount of seeding removal that could occur during set up. Unfortunately this was hampered by software faults. The instrument locked itself down with a full power plasma running and had to be reset, which most likely removed almost all seeding material from the surface, but still allowed for the gathering of valuable information.

Initial observations of silicon substrate (SSi2), upon removal from the instrument, showed a definite change from before the deposition (**Figure 25**). The mirror polish surface had been turned into a matte finish, although some of its mirror either remained or was added from the deposited film. This contrasted greatly to Ex1's SSi1, which was still very reflective and had birefringent properties. **Figure 26** shows the Raman spectrum of SSi2. The shape is similar to those produced from Ex1 but with some significant differences. The 1140 cm⁻¹ peak shows promise of nanocrystalline diamond and this is backed up by a shoulder on the D band, possibly being produced from a crystalline diamond peak at 1132 cm⁻¹. While the majority of the spectrum still points towards amorphous graphitic deposition, there is strong evidence for diamond fabrication, and the start of a proper full scale diamond growth.

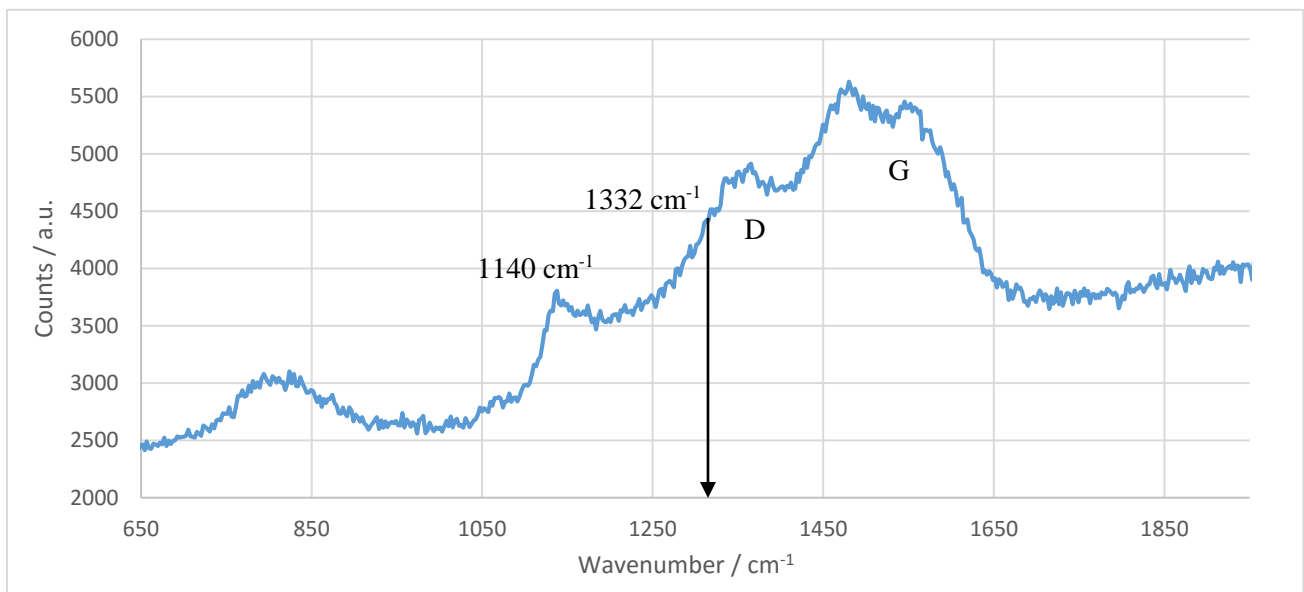


Figure 26. Raman spectrum of SSi2.

^{xvi} 0.75 mm from 0.5 mm.

^{xvii} 0.5 mm from 0.25 mm.

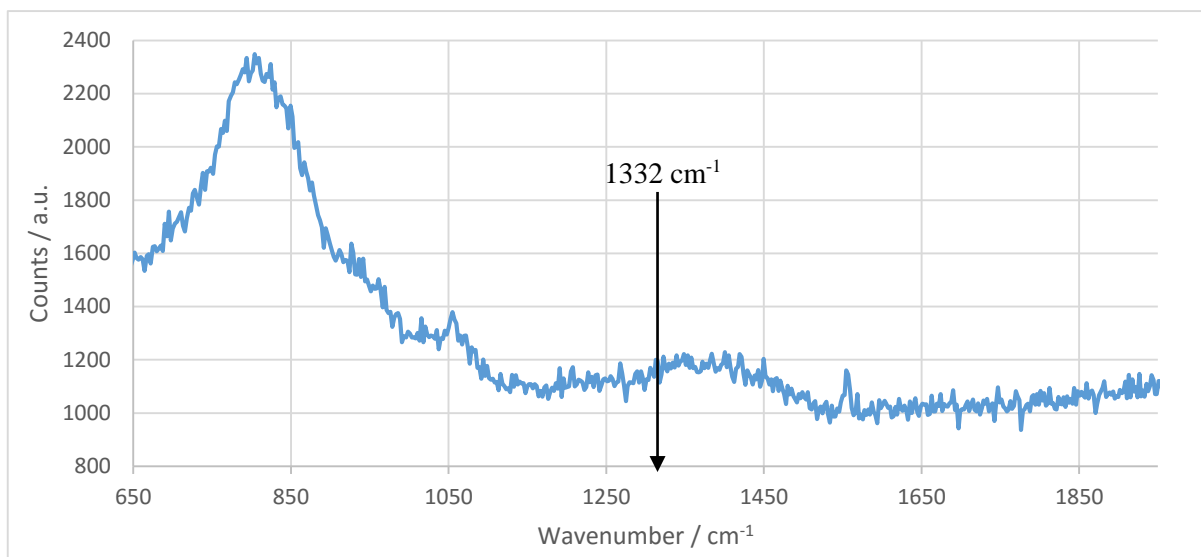


Figure 29. Raman spectrum from SMO2 after deposition.

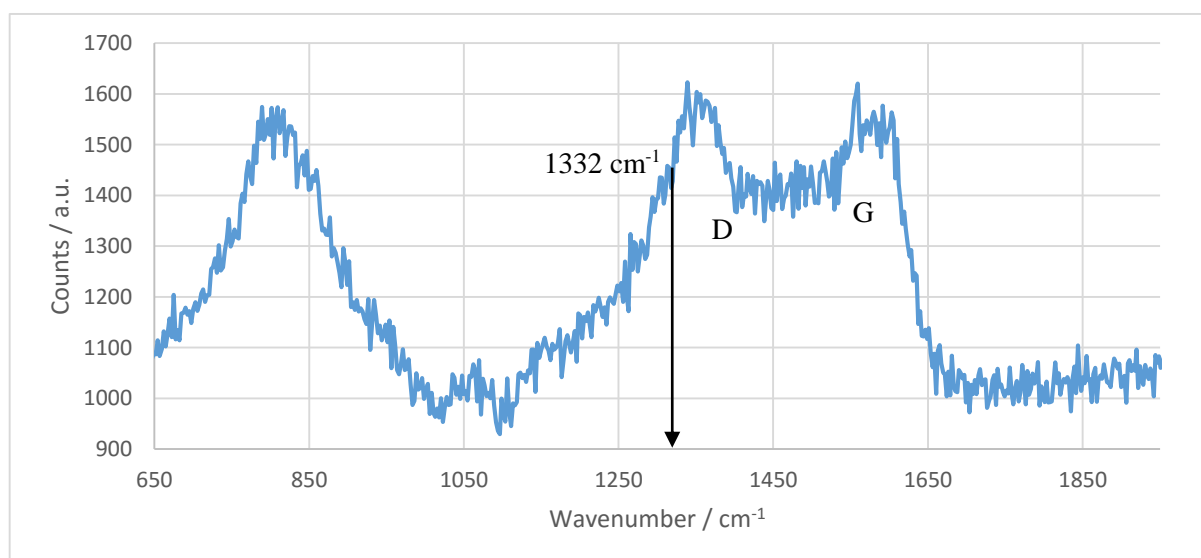


Figure 28. Raman spectrum for SS2 after deposition.

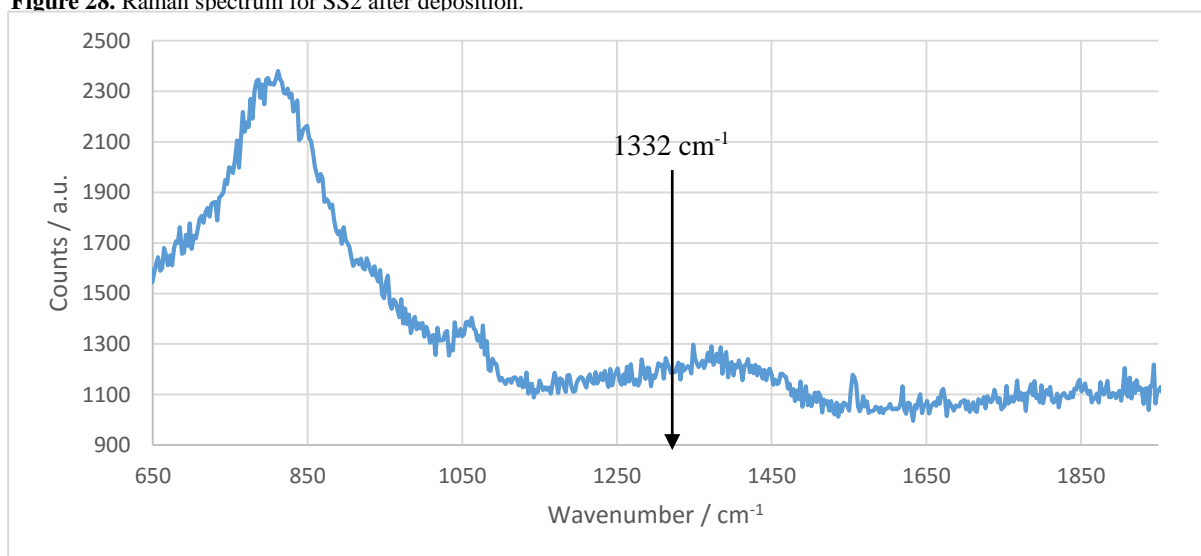


Figure 28. Raman spectrum of an unreacted seeded molybdenum substrate square. No diamond peak is expected but is still noted.

The other deposition surfaces, SMO2 and SS2, unfortunately were not as promising for diamond growth. The molybdenum substrate looked almost unchanged to the eye to the non-reacted substrate. The only noticeable variation being a slightly whiter appearance. However, the seeding solution droplet on the molybdenum deposition plate produced a birefringence pattern and there was promise for some form of deposition upon it (**Figure 25**). The Raman spectrum for these samples (**Figure 27-Figure 29**) unfortunately showed no such promise. The molybdenum square showed almost no growth, with only a small hump in the amorphous graphite/diamond wavenumber range. However, when compared to a non-reacted identical sample the spectra were identical. This is thought to be due to the extended running of a hydrogen only plasma, corroding away the seeding material. This resulting in all the seeded nanodiamonds being removed and no growth seen on the substrate afterwards. Given this result, it is safe to assume that the silicon substrate was also stripped of all seeding material before deposition occurred, which would mean that all deposition occurring on it proceeded on non-seeded silicon. While no deposition occurred on the molybdenum, this result shows promise for repeated growth runs without seeding, even if the substrate has to be changed from molybdenum to silicon for future use.

The SS2 Raman showed almost completely amorphous graphite with no evidence of diamond growth. This was concluded from the absence of both the 1140 cm^{-1} peak and no shoulder being seen on the graphitic D band to hint at possible diamond growth.

The silicon substrate appears to be the preferred growth medium for deposition within the reactor when combining the results from both Ex1 and Ex2. The initial design of the reactor aimed at running mirror polished molybdenum plates. With the need to run at higher than usual temperatures, the deposition plates may have to be altered to silicon plates. While further depositions will have to be run, and higher temperatures may favor molybdenum deposition, initial tests suggest the need for a slight redesign, with an eventual lower operational window.

While further experiments would produce a better understanding of preferred deposition mediums, if the preferred deposition medium remains silicon across these experiments then not only a redesign of the PDC PA-CVD instrument to include silicon plates will be required but an alteration of the Taguchi control values as well. This is due to the temperature values being higher than normal to reflect the higher melting point of molybdenum, with the other parameters having to be altered to reflect these changes. Experiments conducted on silicon will allow for a definitive answer to this question and is the basis for the next experiment.

Ex3

After the preference of deposition on silicon, and the possibility of deposition on non-seeded substrates, a longer strip of silicon was used for Ex3 (**Figure 30**). This was also left unseeded to see if deposition definitely occurred on non-seeded substrates. The length of the silicon was chosen to experiment on any variation in temperature across the substrate surface. With the inclusion of the wire spacers, it was

thought that the conducting wire would alter the surface temperature relative to the center of the plate which would lead to non-uniform deposition.

The set up for this experiment was identical to the previous one. The air leak was still evident in OES spectrum of the plasma system so tests were done by varying the methane concentration to see what effects this had on the CN, C₂, and CH OES peaks. The plasma was also observed to see if a more characteristic green plasma glow could be observed with the addition of enough methane. This led to a long pre-deposition period of varying methane concentrations which may have affected the eventual deposited films quality but to counter this a long hydrogen only plasma was run prior to deposition. All OES spectrum can be viewed in **Figure 32**.



Figure 30. NSSi3 after deposition. The right point was placed at the edge of the molybdenum deposition plate with the straight edge running along the plate's diameter.

Unfortunately due to an issue with the OES collector set up, the spectrums were not taken at a constant point or with constant aperture, so direct comparison is not possible, but valuable data can still be obtained. As seen in **Figure 31**, high levels of methane in the system, equating to 10% methane concentration, produced both CH, at 431 nm, and C₂, at 516 nm, growth species peaks in the system, showing the possibility of high quality growth at these levels. These peaks began appearing at a minimum methane flow rate of 20 sccm, or 4% methane concentration. This shows the limit of growth conditions within the reactor with the air leak still present. Further deposition runs will be conducted at no lower than 4% methane or else the primary growth species will not be present in enough quantities to allow for growth.

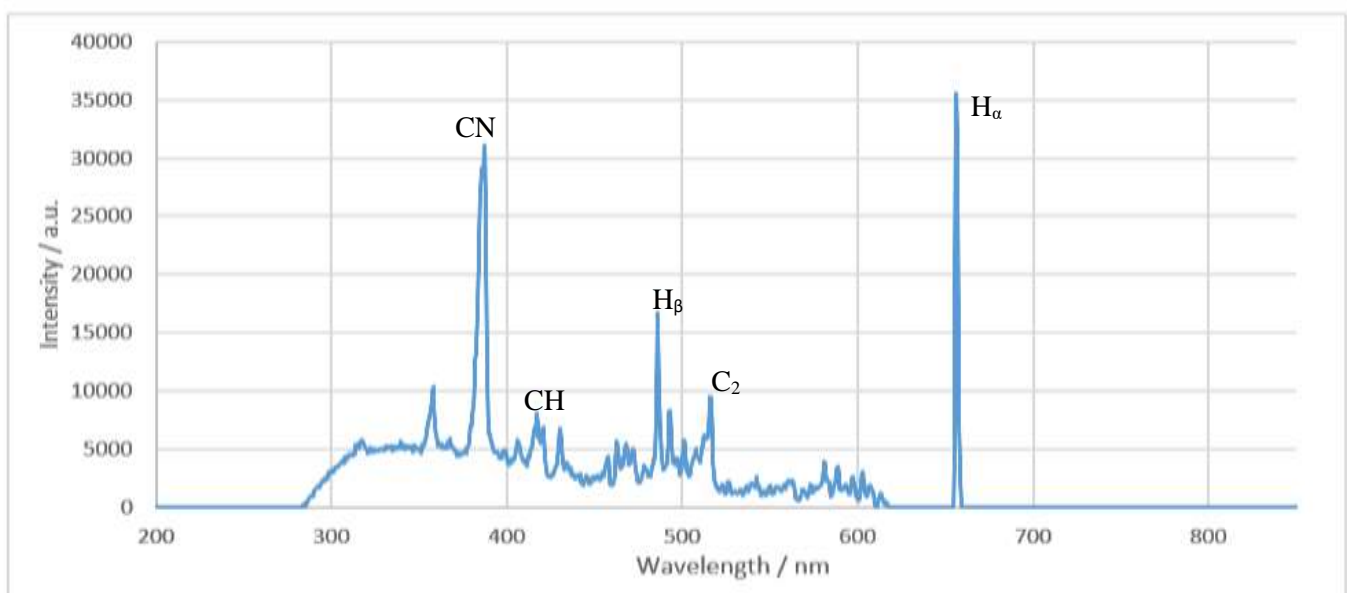


Figure 31. OES of 50 sccm of methane in hydrogen plasma, Ex3.

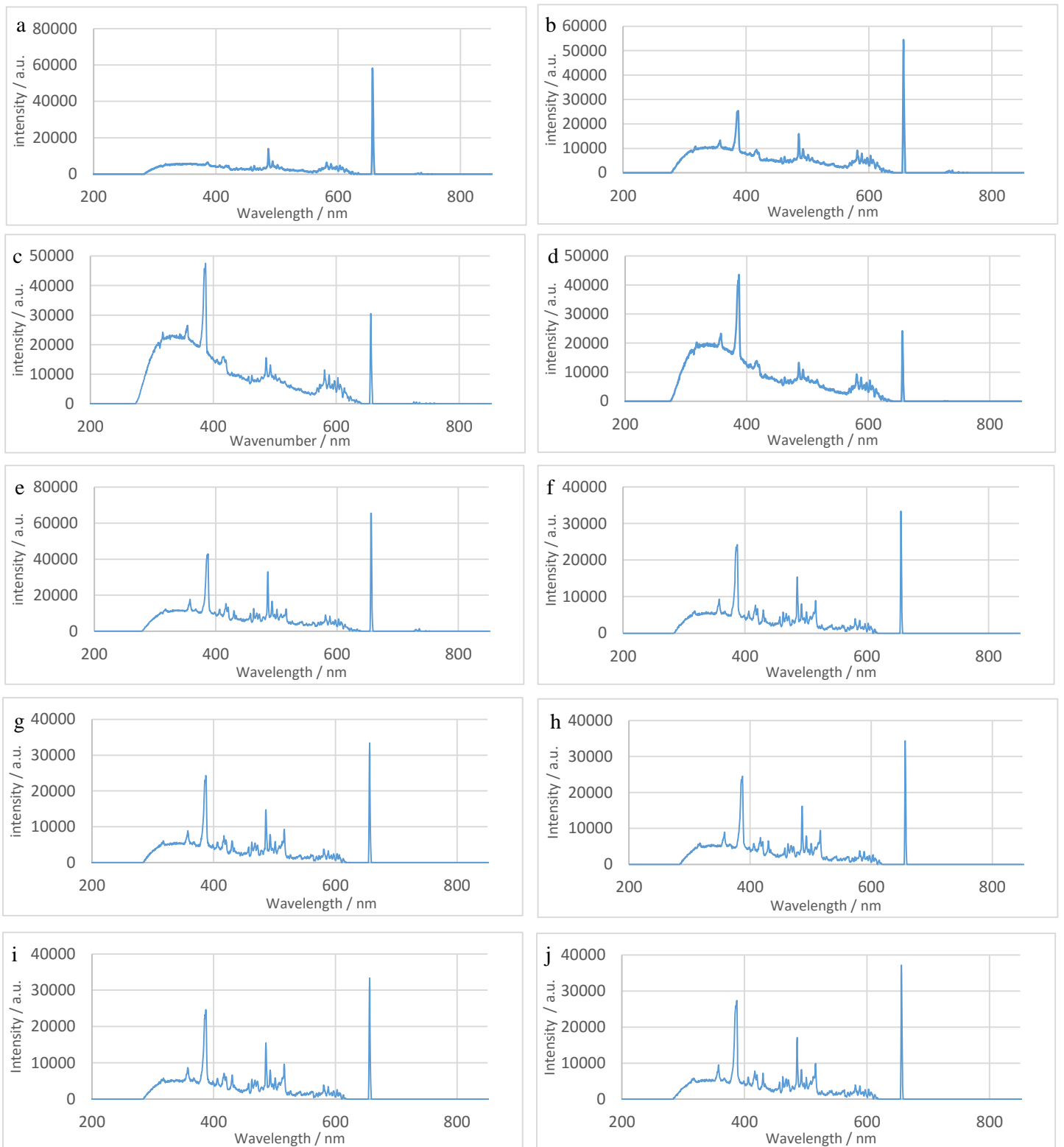


Figure 32. Produced OES spectra from Experiment 3. These were taken from a hydrogen plasma with various percentage additions of methane. Graph a contains 0 sccm methane, b contains 5 sccm, and continuing in 5 sccm steps up to 45 sccm methane in graph j. Peaks labeled α and β correspond to the H α and H β emission line respectively. Peaks labeled CN are due to the CN radical emission and are a result of a nitrogen leak into the system. Peaks with a C $_2$ or CH label are the respective growth species for diamond. If these peaks are not visible on the spectra, an arrow will be printed to show the theoretical location of these peaks. As the concentration of methane in the system increases the strength of the CN emission also increases, with no nitrogen emission visible with no methane present. This shows a nitrogen leak is evident in the methane inlet pipework and is the focus of the investigation into the elimination of methane from the system. What is also seen is the appearance of the main growth species, C $_2$ and CH, at methane concentrations above 4%, or 20 sccm. This shows, while the nitrogen leak is still evident, a minimum methane concentration to allow for growth to occur, as below this level the production of growth species is unfavored compared to the CN radical formation.

Hopefully upon the removal of the air leak, these percentages can be brought lower in order to produce higher quality diamond at a slower rate, but similar tests will have to be taken to ensure when the CH and C₂ species are present.

Initial examinations showed little deposition. The only observable deposition point being a partial finger print mark at the outside edge. This was accidentally placed on the mirror polished substrate face during placement within the chamber. What was observed was the organic matter deposited improving deposition conditions over pure polished silicon. Whether this is due to the introduction of surface defects producing nucleation points or organic matter for seeding material is unknown. Further tests should be conducted on the effect of organic matters on deposition. SEM images of the substrate offer an insight to the type of diamond formed, if any, and highlight the variation in deposition from the center to the edge of the deposition plate.

The SEM showed no variation in nucleation density across the silicon substrate, from the edge of the molybdenum plate to the center. A steady temperature across the substrate is essential for high quality diamond fabrication. Although checks to ensure consistency must be made, temperature variation is not a parameter requiring further investigation at this point.

There was no evidence of any large amount of nucleation away from the edges of the silicon, with a sharp increase in deposition density towards any edge of the substrate (**Figure 33**).

An increase in the plasma field intensity could be the cause. As the electric field reaches the edge of the substrate, the change in the surface morphology naturally leads to an intensification of the field lines. This results in a higher power density nearer the edges and a greater production of deposition radials, increasing nucleation rate and diamond growth.

Further examination of these growth species provided an interesting insight to the product being formed. The spherical shapes, as seen in previous SEM images of SMO1 and SSi1,

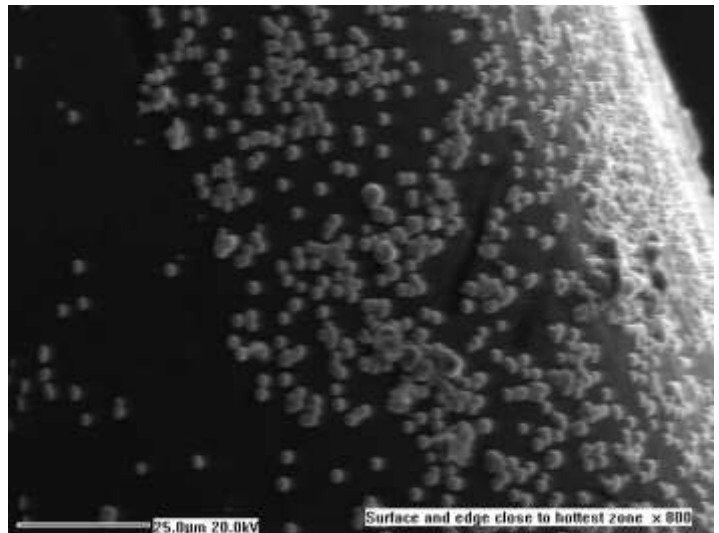


Figure 33. SEM of NSSi3 viewing the edge of the substrate (top right) leading inwards.

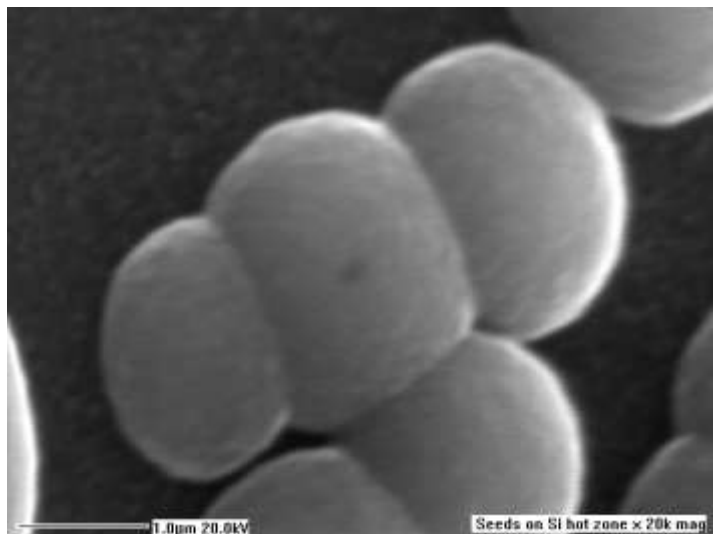


Figure 34. SEM image of a small cluster of deposited ballas diamond on NSSi3.

combined with a scaly surface morphology is characteristic of ballas diamond growth (**Figure 34**). This is characteristic of early stages of similar forms of diamond growth as seen in other DC PA-CVD systems^[7,6,49,50], and is congruent with the eventual growth of nanocrystalline diamond films.

To achieve a full layer of nanocrystalline growth, longer deposition times will allow the newly nucleated diamond particles to grow and join together to form a single layer. Further refinements in the system may also be necessary to allow for either faster growth rates or increased nucleation rates. Only a low nucleation rate was seen on the substrate away from the edges. While the previous samples from Ex2 may have had most of the seeding particles removed from it, a reduced percentage remained to improve deposition rate and this should be further tuned to allow for ideal deposition. A deposition of ballas diamond mainly occurs when methane concentrations are too high or plasma intensities are too low^[82]. By increasing the plasma intensity, and lowering the methane concentration, facet diamond growth should be observed in the next run.

Taguchi optimization relies on minimizing the number of variables that are not under direct control of the operator. By eliminating the possibility of variation in substrate temperature across the deposition surface, it will allow for greater control over the final product, along with reducing the time dedicated to controlling this factor. While only a small factor in the overall PDC PA-CVD instrument it greatly reduces the possible variation in results that could be seen across the produced films, especially when conduction experiments at the limits of the diamond fabrications window.

Ex4

The final deposition run conducted was conducted with increased wire spacing to further increase the operating windows. This also allow for the recreation of an initially untested factor in the Lux *et al.*^[49] paper. This factor was the cathode temperature, and the need for it to be within a certain range to allow for non-graphitic deposition to occur. This was initially not considered due to the limitations of the current instruments set up, no deposition occurring on the cathode surface and also due to the other DC PA-CVD systems^[2,6,7,50] not stating the importance of cathode temperature.

The wire spacing on the cathode was changed from the 0.5 mm tantalum wire to a 0.75 mm tungsten wire, while the substrate accommodated a 1 mm tungsten wire, from its original 0.75 mm tungsten wire. This allowed satisfactory substrate temperatures to be reached.



Figure 35. Produced films from Ex4 showing SSi4 and the molybdenum deposition plate.

Additionally, a cathode glow was achieved at deposition conditions, raising its temperature to $\sim 650\text{ }^{\circ}\text{C}$. Deposition was also conducted with a minimal, hydrogen only, plasma pre-running, allowing for the substrate to remain as close to the intended seeding condition as possible.

Upon removal of the substrate from the reactor it was immediately obvious that the increase in cathode temperature had improved the performance of the system. What can be seen is clear birefringence not only on the substrate itself but also the molybdenum plate (**Figure 35**). This was a similar finish to that seen on SMO1 but with added birefringence effect. The deposition directly onto the molybdenum plate was also new to this experiment. The same plate was used for all experiments as no deposition had been produced on it during any previous experiments (the SS2 droplet can be seen as a grey smudge

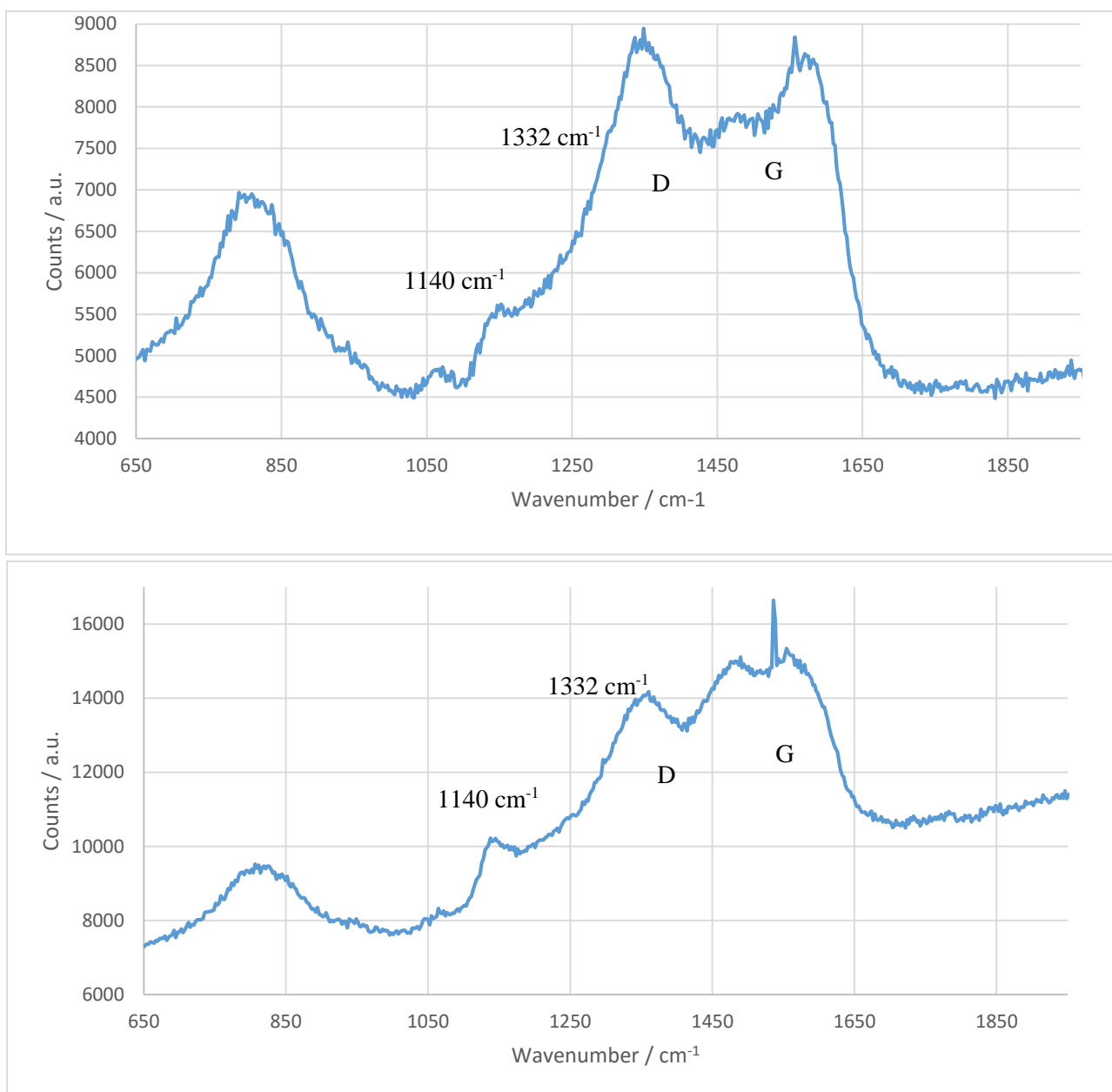


Figure 36. Raman spectrums of SSi4 (top) and the molybdenum plate (bottom).

bottom left of the plate). An increase in the cathode temperature allowed for rapid deposition onto this surface.

Raman spectroscopy for the two surfaces, SMO4 and the molybdenum plate, show similarities to SSi2 (**Figure 36**). While both still show strong graphitic D and G bands they also contain the 1140 cm^{-1} peak along with 1332 cm^{-1} shoulders. The sharp peak on the molybdenum plate at 1538 cm^{-1} could not be identified in the literature^{xviii}. This peak was not seen on other deposition runs and was evident regardless of where on the molybdenum the Raman spectrum was taken. It is possible that it was due to a contaminant on the molybdenum substrate, due to its rough handling throughout construction and initial tests^{xix}, but its origin is unknown and further examination must be done to find its source.

SEM images of the substrate^{xx} showed a rough and non-identifiable layer (**Figure 37**). The SEM instrument was not powerful enough to produce a detailed image of the surface and while many features are evident their exact natures are unclear. There is apparent growth along defects and scratches on the initial substrate, leading to the wide range of shapes and structures seen, and the rapid growth seen, when compared to the other samples produces from Ex1-3 under the SEM.

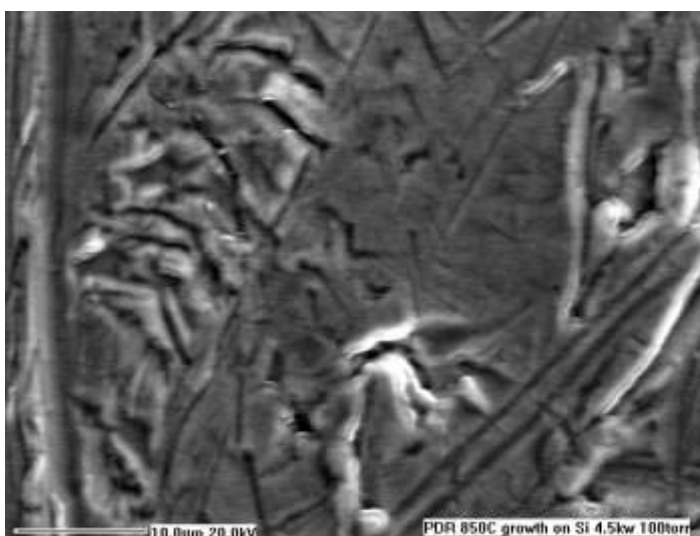


Figure 37. SEM image of SMO4.

As **Figure 38, left image**, shows, the produced layer is very thick and uniform relative to other deposition runs, with a few micrometers of growth evident in the SEM images. While no individual diamond crystals are evident, definite ballas diamond growth can be seen in **Figure 38, right image**, with the scaly surface evident in the lower right hand side of the image. This shows definite nanocrystalline growth of diamond has been achieved. This is further backed up with the appearance again of the spherical growth, showing that seeding commenced as before, yet growth rates were enough to allow for full coagulation and film formation.

The production of a continuous diamond layer suggests suitable conditions for full diamond synthesis. Looking at the substrate, and in comparison to the other produced substrates, the appearance of a more matte finish to the deposited substrate is promising for growth, and should be looked for in final products for quick evaluation. However, this evidence is not conclusive of a successful deposition run.

^{xviii} No literature papers gave spectrums with peaks either matching up with the peaks wavenumber or being produced from plausible compounds.

^{xix} As these molybdenum plates are intended as placeholders until the polished plates are introduced for optimization.

^{xx} The molybdenum plate was too large to be examined by SEM.

Further work will have to be done to analyze the deposited film on the molybdenum plate, and a cleaning system will have to be devised as further deposition runs will be depositing films on the substrate plate continually.

Because of the completion of experiments for this report valuable information has been learnt about the limits of the instrument, and this will be reflected when updating the Taguchi system for future optimization. The rapid increase in growth seen in Ex4, due to the increase in the cathode temperature, has shown a vital aspect for successful deposition. It has shown to be essential for the Taguchi optimization to include this factor into the matrix. Due to most DC PA-CVD instruments in the literature using the same temperature for both the cathode and substrate [2,6,7,49,50], this will be incorporated into the Taguchi matrix by using the same substrate temperature for both the substrate and the cathode, therefore allowing this factor to be included without an entire Taguchi redesign.

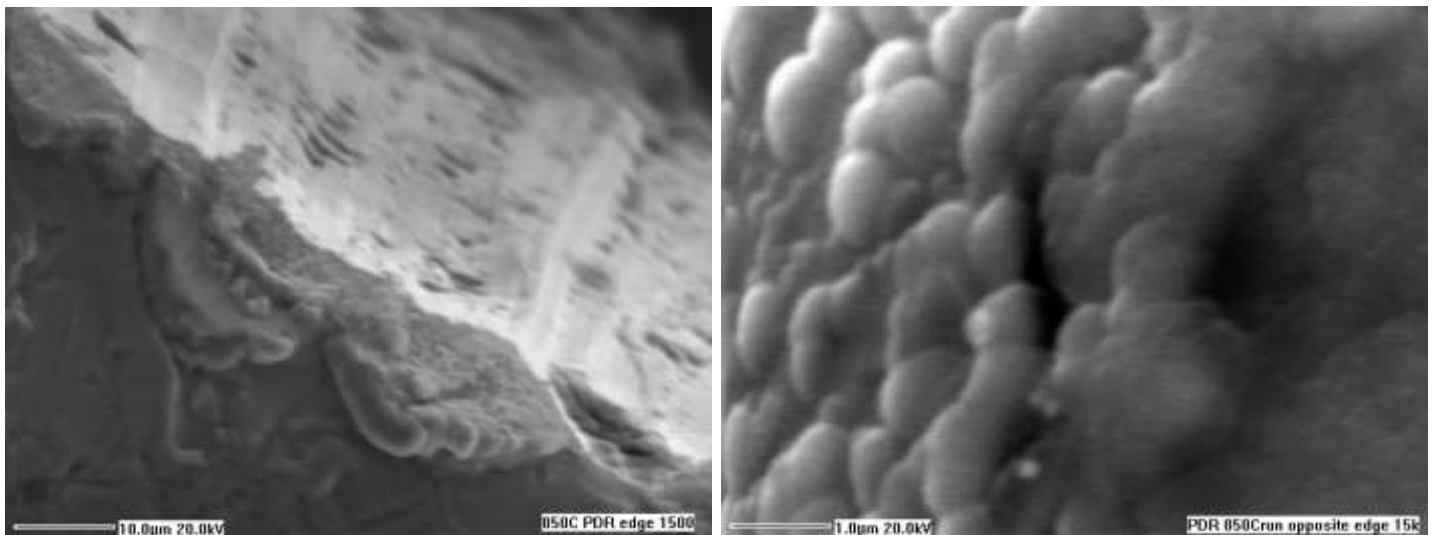


Figure 38. SEM image of SMO4. Left image: the deposited film is in the bottom left, with the change in color in the middle dictating the start of the silicon substrate. Right image: ballas diamond growth is evident with the scaly surface shown in the bottom right of the image, along with the spherical diamond nucleation sites, growing off the side of the film, visible in the top left.

Chapter 6: Conclusions and Future Research

While the nitrogen leak is still affecting the growth of the diamond films, and several other factors have to be brought under control, full diamond deposition runs and instrument optimization are not far away.

The inherent advantages that this instrument has over other CVD systems are evident. The inherent plasma stability evidenced will allow for reproducible deposition runs, with the computer control system being implemented to allow for precise extended runs with minimal input. Even striking the plasma is conducted with minimal effort expended into controlling the reactors deposition conditions. The ‘Goldilocks’ zone of control will also be easier to adhere to upon automation, reducing the only cause of instability in the plasma: the arcing or partial coverage from improper conditions.

Deposition runs have shown that diamond fabrication is possible. Ballas diamond has been created on several deposition runs, with these formations being linked to systems with too low power or too high

methane concentrations^[82] or with improper temperature set ups^[81]. These can be corrected and will result in optimization within the system, providing directions for further tests, and a window in to the final operational range of the machine. With most graphitic ballas deposition occurring at 5% methane, deposited with 4.75 kW power, this can be set as the upper limit of methane concentration without greatly increasing the power. An increase in power is within the limits of the instruments power supply, but with the current set up producing bumping in the cooling system at powers much above 5 kW, this will have to be rectified before any higher power runs can commence.

Running the instrument at higher voltages may also produce further issues as the feedthrough system's limits under its current configuration are unknown. While no issues have been experienced at 5 kW, an increase in power, and therefore voltage, will always bring with it an increased risk of an insulator breakdown. The down time, mainly due to the redesign and production of a new feedthrough, will delay any work. If this issue occurs during optimization, even with the great reproducibility of deposition conditions, the results may be skewed. With possible weeks of work needed to repair the instrument, environmental changes may lead to an altered deposition system within the instrument.

Nitrogen addition has been shown to produce poor quality films, but also has shown to increase the growth rate of diamond by a factor of two.^[99] Taking this into consideration, and with the best growth observed on Ex4's SMO4 sample being $\sim 10 \mu\text{m h}^{-1}$ (**Figure 39**), it can be calculated that pure diamond growth rate with no nitrogen leak present could realistically be $\sim 5 \mu\text{m h}^{-1}$. While this may appear low, further optimization will result in much faster growth rates. Although absolute maximum growth rates will come with a decrease in diamond quality, overall maximums should be investigated for full understanding of the PDC PA-CVD's abilities.

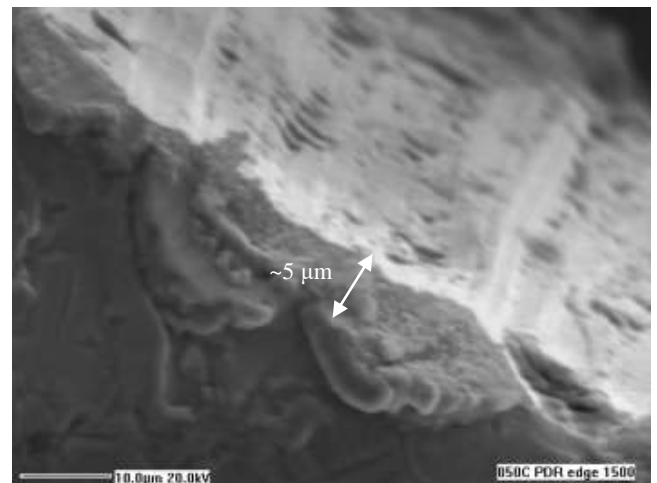


Figure 39. SEM image of the edge of SMO4, showing the thickness of the deposited film.

The results presented above point to the beginning of a new type of diamond depositing instrument, offering a quick turnaround, high quality fabrication (of either ballas or possibly large crystal diamond), and easily reproducible depositions. Upon optimization the purpose of the instrument is to produce films of either ^{12}C or ^{13}C diamond, with discrete layers as thin as possible, able to be utilized for further work with either thermal, optical or doping. The only full film deposition run conducted produced a roughly textured surface with little uniformity. But it is a promising sign that these features appeared to follow initial faults in the substrate surface. Upon the start of proper production experiments, a mirror-polished molybdenum cathode and substrate will be installed. This will allow for easy removal of any produced diamond films, and with almost no surface features which could transfer to the grown film,

the theoretical production of smooth and even surfaces is expected. This combined with the ballas diamond growth, will allow for very small layer boundaries to be formed. Further research will be necessary to determine if this is possible. Because of the inherently small crystal size of Ballas diamond, there will be little variation in the surface height across the diamond, which would allow for an overall shrinking of the diamond layers and an improvement in packing of the isotopically pure layers.

Further Research

Because of the limited running of the new PDC PA-CVD instrument during the project timeline, due to the various delays and issues discussed above, there is wide scope for future work. This will then be followed by a more long term aim of the instrument with the focus of producing isotropic layers of high quality diamond films.

Immediate Research

Briefly touched upon in various sections of the Results and Discussion section, these experiments will extend on from completed run depositions and will aim to correct some of their issues and poor results to achieve diamond deposition of a semi-high quality in a single uniform film.

The most pressing issue is to resolve is the air leak in the system. The leak is reducing the quantity of C_2 and CH radicals^[76], and thus reducing growth rates, and is also damaging deposited diamond growth which is reducing overall quality of produced diamond^[64]. Initially all linkages in the gas flow pipes were tightened and checked which helped reduce the base pressure of the system by ~90% but OES spectrum of a methane/hydrogen plasma still showed a prominent CN peak at 388 nm. A fault in the methane Mass Flow Controller (MFC) connection point was identified and a replacement component was installed, yet the issue persisted. At the time of writing no further modifications have been undertaken. The next step will be to replace the methane MFC with another MFC to see if the connection point on the MFC is the issue. While this will not allow for accurate gas flow control, it will allow the methane MFC to be ruled out as the problem.

Once this issue has been resolved, the next avenue of research will be the improvement of the deposited films. Upon proper heating of the top electrode, the rate of deposition was greatly increased and ballas diamond films were produced. An accurate reading of the temperature of both the top and bottom electrode will be essential for validating future runs and thermocouples will need to be reinstalled on the substrate and installed along the cathode. With the change in design due to the wire addition, the actual installation of the cathodes may prove difficult but could be circumvented with the acquisition of a reliable and wide temperature range pyrometer, one for each surface. An increase in the thickness of the wire around the cathode will also be essential to allow for greater temperatures to be achieved without overheating the cooling system

With the bulk of the optimization to be done by the Taguchi optimization, the range of the parameters suggested can be checked with small deposition runs. Evidence of pure diamond formation will need to be observed to allow for a presumption on what the ideal parameters are.

Ex4 showed the growth of ballas diamond and this has been linked with both a too high concentration of methane and a too high deposition temperature^[81]. These experiments were run on Microwave Plasma Assisted CVD (MPACVD) systems and therefore cross comparisons are not completely transferable. While the concentration of methane can draw immediate comparisons, the power output of the instrument was only 1.4 kW, compared to 4.75 kW on this system. As *Haubner and Lux* showed^[82], an increase in power results in a decrease of ballas diamond growth. While this was also conducted on a similar MPACVD system, it can be safely concluded that running an experiment at lower methane concentrations may result in higher quality diamond, especially as other DC PA-CVD systems^[6,7,49,50] all have methane concentrations roughly in the 3-4% range. This may lower overall growth rates but will allow for initial diamond fabrication.

Higher temperatures may not necessarily produce better diamond. While it should be explored in future work after initial optimization, initially the temperatures should be kept to a maximum of 1000 °C, as long as the cathode and substrate are showing similar temperatures. This appears to be a major factor for ideal deposition. The substrate temperature necessity is widely known from both the MPACVD systems as well as the Hot Filament CVD (HFCVD) system, both require heat to be inducted into the system to allow for proper deposition. Little is known about how the temperature of the cathode affects growth conditions. *Lux et al.*^[49] even stated that if the cathode temperature was not between 900-1000 °C then only graphitic depositions should be expected, but made no remark on the effects of substrate temperature.

Little experimentation with pressure has been conducted and obviously will be essential to future depositions. However, because the current value of ~100 Torr is used as both the standard in this instrument and other papers, sticking to this value will be ideal to allow minimal variables for initial diamond fabrication.

No papers have been found that experiment with varying the flow rates of the gasses. While varying the flow rate may have little effect on the production of diamond it should eventually be explored to allow full understanding of all the instruments capabilities.

To provide the best hope of pure diamond fabrication, runs should be conducted under standard operating conditions. Experiments of ~4% methane with powers ~5 kW providing substrate and cathode temperatures of ~800-900 °C at ~100 Torr will be the main aim. Factors where little knowledge on their effects of diamond growth of quality, such as the pulse frequency or the gas flow rate, should be kept at a constant value.

Long Term Aims

Upon correcting the current issues with the PDC PA-CVD system, along with the initial Taguchi optimization, the instrument will be producing high quality diamond films quickly and reproducibly. To increase the instruments abilities a second round of Taguchi optimization may be explored. Some variables are not fully optimized yet (gas flow rate, plate distance etc.) while other parameters require further experimentation into their limits (high plate temperature, high pressure etc.). All of these new parameters could all be addressed with this second Taguchi optimization. But immediate results could be explored with simple small scale optimization. While the Taguchi method will allow the creation of high quality diamond films, more exact effects could be explored by altering the variables by smaller increments than in the optimization process. For example; by altering the pressure by increments of 10 Torr around the optimized pressure it can not only be shown that this is the ideal level, but it would also be possible to observe the effects of the pressure at that level and how these effects affect quality. This can be done across all parameters and will allow further minute refinements of the system.

These can then be built upon through the creation of phase diagrams for fabrication. By creating similar systems to Bachmann *et al.*^[94], and utilizing any grouping of parameters, one can create a simple production graph for any form of required film. This could be used to quickly and easily set up the instrument for any form of diamond chosen to be produced, from ballas to single crystal.

When full control over the instrument has been achieved exact production of isotopically pure layers can be explored. The main issue will be the reduction of the boundary layer. This can be explored through altering the cycle time between removal of normal methane and the introduction of isotopically pure methane. Care will have to be taken to ensure correct deposition continues while the methane levels drop in the chamber. This could be avoided through two possible methods. Firstly, by introducing the ¹³C methane earlier, which may limit the thickness of the boundary layer but would allow for even deposition to continue. Or secondly, allowing a hydrogen only plasma to run for a specific amount of time between changing methane sources to remove any poor deposits formed upon the drop in methane concentration leading to two distinct layers being formed, but may result in poor quality diamond at the film surface. This in turn could lead to poor cohesion between the isotopically different films. The hydrogen plasma portion of the deposition could also increase the roughness of the primary film surface, resulting in a larger boundary layer through the larger physical size of the diamond crystals at the interval increasing the required boundary layer thickness needed for distinct layers to be formed.

These tests will also have to include further work with doping of the diamond layers. This research remains for the future, with the great majority of the current work being dedicated for optimization and boundary layers to allow for the incorporation of dopants into an ideal system, and to determine how they affect the grown film. But with all the prior knowledge gained these effects should be easy to counter through simple use of produced phase diagrams and Taguchi optimization.

References

1. S. Lee, Z. Lin and X. Jiang, *Materials Science and Engineering: R: Reports*, 1999, 25, 123-154.
2. K. Suzuki, A. Sawabe and T. Inuzuka, *Jpn. J. Appl. Phys.*, 1990, 29, 153-157.
3. S. Koizumi, T. Murakami, T. Inuzuka and K. Suzuki, *Appl. Phys. Lett.*, 1990, 57, 563.
4. K. Kurihara, K. Sasaki, M. Kawarada and N. Koshino, *Appl. Phys. Lett.*, 1988, 52, 437.
5. K. Suzuki, A. Sawabe, H. Yasuda and T. Inuzuka, *Appl. Phys. Lett.*, 1987, 50, 728.
6. W. Lee, Y. Baik and K. Chae, *Thin Solid Films*, 2003, 435, 89-94.
7. K. Chae, Y. Baik, J. Park and W. Lee, *Diamond and Related Materials*, 2010, 19, 1168-1171.
8. N. Ali, V. Neto, S. Mei, G. Cabral, Y. Kousar, E. Titus, A. Ogwu, D. Misra and J. Gracio, *Thin Solid Films*, 2004, 469-470, 154-160.
9. M. Elliott, P. May, J. Petherbridge, S. Leeds, M. Ashfold and W. Wang, *Diamond and Related Materials*, 2000, 9, 311-316.
10. J. Ma, M. Ashfold and Y. Mankelevich, *Journal of Applied Physics*, 2009, 105, 043302-1.
11. T. Vandeveld, T. Wu, C. Quaezhaegens, J. Vlekken, M. D'Olieslaeger and L. Stals, *Thin Solid Films*, 1999, 340, 159-163.
12. J. Wang, *Xian dai re li xue*, Fu dan da xue chu ban she, Shanghai, 2010.
13. L. Martin and M. Hill, *Journal of Materials Science Letters*, 1990, 9, 621-623.
14. C. Chu, M. D'Evelyn, R. Hauge and J. Margrave, *Journal of Materials Research*, 1990, 5, 2405-2413.
15. S. Harris and L. Martin, *Journal of Materials Research*, 1990, 5, 2313-2319.
16. Y. Liu, C. Liu, Y. Chen, Y. Tzeng, P. Tso and I. Lin, *Diamond and Related Materials*, 2004, 13, 671-678.
17. D. Zhou, T. McCauley, L. Qin, A. Krauss and D. Gruen, *J. Appl. Phys.*, 1998, 83, 540.
18. C. Corbella, E. Pascual, M. Gómez, M. Polo, J. García-Céspedes, J. Andújar and E. Bertran, *Diamond and Related Materials*, 2005, 14, 1062-1066.
19. M. Phadke, *Quality engineering using robust design*, Prentice Hall, Englewood Cliffs, N.J., 1989.
20. J. Rosa, A. Robin, M. Silva, C. Baldan and M. Peres, *Journal of Materials Processing Technology*, 2009, 209, 1181-1188.
21. R. Rao, R. Prakasham, K. Prasad, S. Rajesham, P. Sarma and L. Rao, *Process Biochemistry*, 2004, 39, 951-956.
22. P. Selden, *Sales Process Engineering: a Personal Workshop*, ASQ Quality Press, Milwaukee, 1996.
23. D. Liu and Y. Cai, *IEEE Trans. Power Syst.*, 2005, 20, 2006-2014.
24. N. Daneshvar, A. Khataee, M. Rasoulifard and M. Pourhassan, *Journal of Hazardous Materials*, 2007, 143, 214-219.
25. A. Cheeseman, PhD, University of Bristol, 2006.

26. N. Ali, V. Neto, S. Mei, G. Cabral, Y. Kousar, E. Titus, A. Ogwu, D. Misra and J. Gracio, *Thin Solid Films*, 2004, 469-470, 154-160.
27. E. Salgueiredo, M. Amaral, M. Neto, A. Fernandes, F. Oliveira and R. Silva, *Vacuum*, 2011, 85, 701-704.
28. *Tlchm.bris.ac.uk*, 2015.
29. A. Dean and R. Unal, 1991.
30. J. Field, *The Properties of natural and synthetic diamond*, Academic Press, 1992.
31. R. Davis, *Diamond films and coatings*, Noyes Pub., Park Ridge, N.J., 1993.
32. M. Prelas, G. Popovici and L. Bigelow, *Handbook of industrial diamonds and diamond films*, Marcel Dekker, New York, 1998.
33. J. Wilks and E. Wilks, *Properties and applications of diamond*, Butterworth-Heinemann, Oxford, 1991.
34. A. Gicquel, K. Hassouni, F. Silva and J. Achard, *Current Applied Physics*, 2001, 1, 479-496.
35. D. Pofperl, *J. Appl. Phys.*, 1973, 44, 1428.
36. S. Hay, W. Roman and M. Colket, *Journal of Materials Research*, 1990, 5, 2387-2397.
37. S. Chauhan, *J. Appl. Phys.*, 1976, 47, 4746.
38. A. Sawabe and T. Inuzuka, *Appl. Phys. Lett.*, 1985, 46, 146.
39. K. Hirabayashi, Y. Taniguchi, O. Takamatsu, T. Ikeda, K. Ikoma and N. Iwasaki-Kurihara, *Appl. Phys. Lett.*, 1988, 53, 1815.
40. S. Iijima, Y. Aikawa and K. Baba, *Appl. Phys. Lett.*, 1990, 57, 2646.
41. R. Buckley, T. Moustakas, L. Ye and J. Varon, *J. Appl. Phys.*, 1989, 66, 3595.
42. J. Kim, M. Kim, S. Park and J. Lee, *J. Appl. Phys.*, 1990, 67, 3354.
43. L. Robins, E. Farabaugh and A. Feldman, *Journal of Materials Research*, 1990, 5, 2456-2468.
44. Y. Liou, A. Inspektor, R. Weimer and R. Messier, *Appl. Phys. Lett.*, 1989, 55, 631.
45. K. Kobashi, K. Nishimura, Y. Kawate and T. Horiuchi, *Phys. Rev. B*, 1988, 38, 4067-4084.
46. M. Kamo, Y. Sato, S. Matsumoto and N. Setaka, *Journal of Crystal Growth*, 1983, 62, 642-644.
47. S. Matsumoto, *Journal of Materials Science Letters*, 1985, 4, 600-602.
48. H. Yoneda, K. Ueda, Y. Aikawa, K. Baba and N. Shohata, *Appl. Phys. Lett.*, 1995, 66, 460.
49. P. Hartmann, R. Haubner and B. Lux, *Diamond and Related Materials*, 1996, 5, 850-856.
50. H. Lee, H. Jeon and W. Lee, *J. Appl. Phys.*, 2011, 109, 023303.
51. Y. Han, Y. Kim and J. Lee, *Thin Solid Films*, 1997, 310, 39-46.
52. M. Kang, W. Lee and Y. Baik, *Thin Solid Films*, 2001, 398-399, 175-179.
53. I. Raizer, *Gas discharge physics*, Springer-Verlag, Berlin, 1991.
54. B. Sun, X. Zhang and Z. Lin, *Phys. Rev. B*, 1993, 47, 9816-9824.
55. B. Waclawski, *J. Vac. Sci. Technol.*, 1982, 21, 368.
56. T. Anthony, *Vacuum*, 1990, 41, 1356-1359.
57. F. Paschen, *Ann. Phys.*, 1889, 273, 69-96.

58. M. Lieberman and A. Lichtenberg, *Principles of plasma discharges and materials processing*, Wiley, New York, 1994.
59. R. Tsang, C. Rego, P. May, J. Thumim, M. Ashfold, K. Rosser, C. Younes and M. Holt, *Diamond and Related Materials*, 1996, 5, 359-365.
60. C. Yan and Y. Vohra, *Diamond and Related Materials*, 1999, 8, 2022-2031.
61. P. May, P. Burridge, C. Rego, R. Tsang, M. Ashfold, K. Rosser, R. Tanner, D. Cherns and R. Vincent, *Diamond and Related Materials*, 1996, 5, 354-358.
62. Y. Muranaka, *Journal of Vacuum Science & Technology A: Vacuum, Surfaces, and Films*, 1991, 9, 76.
63. S. Harris and A. Weiner, *Appl. Phys. Lett.*, 1989, 55, 2179.
64. Y. Liou, A. Inspektor, R. Weimer, D. Knight and R. Messier, *Journal of Materials Research*, 1990, 5, 2305-2312.
65. L. Zeng, H. Peng, W. Wang, Y. Chen, D. Lei, W. Qi, J. Liang, J. Zhao, X. Kong and H. Zhang, *J. Phys. Chem. C*, 2008, 112, 1401-1406.
66. R. Massalski, *Binary Alloy Phase Diagrams*, American Society For Metals, Metals Park, OH, 1986.
67. E. Smith and G. Dent, *Modern Raman spectroscopy*, J. Wiley, Hoboken, NJ, 2005.
68. S. Praver and R. Nemanich, *Philosophical Transactions of the Royal Society A: Mathematical, Physical and Engineering Sciences*, 2004, 362, 2537-2565.
69. A. Ferrari, *Diamond and Related Materials*, 2002, 11, 1053-1061.
70. G. Balestrino, M. Marinelli, E. Milani, A. Paoletti, I. Pinter, A. Tebano and P. Paroli, *Appl. Phys. Lett.*, 1993, 62, 879.
71. P. Atkins and J. De Paula, *Atkins' Physical Chemistry*, Oxford university Press, Oxford, 9th edn., 2010.
72. S. Fraley, M. Oom, B. Terrien and j. Zalewski, *The Michigan Chemical Process Dynamics and Controls Open Text Book*, 2nd edn., 2006.
73. *Pchemlabs.com*, 2016.
74. *Landinst.com*, 2016.
75. *Ocean Optics*, 2016.
76. K. Clay, S. Speakman, G. Amaratunga and S. Silva, *Journal of Applied Physics*, 1996, 79, 7227-7233.
77. R. Nemanich, *Journal of Vacuum Science & Technology A: Vacuum, Surfaces, and Films*, 1988, 6, 1783.
78. A. Ferrari and J. Robertson, *Phys. Rev. B*, 2000, 61, 14095-14107.
79. H. Kuzmany, R. Pfeiffer, N. Salk and B. Günther, *Carbon*, 2004, 42, 911-917.
80. *Lesker.com*, 2016.

81. S. Bühlmann, E. Blank, R. Haubner and B. Lux, *Diamond and Related Materials*, 1999, 8, 194-201.
82. R. Haubner and B. Lux, *International Journal of Refractory Metals and Hard Materials*, 2002, 20, 93-100.
83. F. Klabunde, M. Löhmann, J. Bläsing and T. Drüsedau, *J. Appl. Phys.*, 1996, 80, 6266.
84. *Uk.airliquide.com*, 2016.
85. *BOConline UK*, 2016.
86. R. Davis, *Diamond Films and Coatings*, Noyes Publications, New Jersey, 1992.
87. D. Liu, H. Sun, J. Pomeroy, D. Francis, F. Faili, D. Twitchen and M. Kuball, *Appl. Phys. Lett.*, 2015, 107, 251902.
88. E. Edelman, P. Seifert, A. Groothuis, A. Morss, D. Bornstein and C. Rogers, *Circulation*, 2001, 103, 429-434.
89. P. Nistor, P. May, F. Tamagnini, A. Randall and M. Caldwell, *Biomaterials*, 2015, 61, 139-149.
90. S. Mandal, T. Bautze, O. Williams, C. Naud, E. Bustarret, F. Omnès, P. Rodière, T. Meunier, C. Bäuerle and L. Saminadayar, *ACS Nano*, 2011, 5, 7144-7148.
91. *Seki Diamond Systems*, 2016.
92. N. Tokuda, *Topics in Applied Physics*, 2014, 1-29.
93. S. Matsumoto, Y. Sato, M. Tsutsumi and N. Setaka, *J Mater Sci*, 1982, 17, 3106-3112.
94. P. Bachmann, D. Leers and H. Lydtin, *Diamond and Related Materials*, 1991, 1, 1-12.
95. *Jeolusa.com*, 2016.
96. *R. plc, Renishaw.com*, 2016.
97. C. Kennedy and G. Kennedy, *J. Geophys. Res.*, 1976, 81, 2467-2470.
98. A. Badzian, T. Badzian, R. Roy, R. Messier and K. Spear, *Materials Research Bulletin*, 1988, 23, 531-548.
99. A. Chayahara, Y. Mokuno, Y. Horino, Y. Takasu, H. Kato, H. Yoshikawa and N. Fujimori, *Diamond and Related Materials*, 2004, 13, 1954-1958.

Table 6, the best depositions conditions for DC PA-CVD systems collected from several literature sources^{2,6,7,49,50}.

Paper Name	Deposition of thick diamond film by pulsed d.c. glow discharge CVD.	Ultranano-crystalline diamond film deposition by direct-current plasma assisted chemical vapor deposition using hydrogen-rich precursor gas in the absence of the positive column.		The 8-inch free-standing CVD diamond wafer fabricated by DC-PACVD.	Diamond thick film deposition in wafer scale using single cathode direct current plasma assisted chemical vapor deposition.	Growth of diamond film by dc plasma chemical vapor deposition and characterization of the plasma.
Paper Reference	P. Hartmann, R. Haubner, B. Lux, <i>Diam. Relat. Mater.</i> , 5 , 1996, 850-856. (4% CH ₄)	L., Hak-Joo, J., Hyeongtag, L., Wook-Seong, <i>J. Appl. Phys.</i> , 109 , 2011, 023303-1. a (H ₂ Rich) b (Ar Rich)		C., Ki-Woong, B., Young-Joon, P., Jong-Keuk, L., Wook-Seong, <i>Diam. Relat. Mater.</i> , 19 , 2010, 1168-1171.	L., Wook-Seong, B., Young-Joon, C., Ki-Woong, <i>Thin Solid Films</i> , 435 , 2003, 89-94.	K. Suzuki, A. Sawabe, T. Inuzuka, <i>Jpn. J. Appl. Phys.</i> , 29 , 1, 1990, 153-157.
Set Up/Strike Conditions	Evacuated to 0.01 Torr but is an old system so may have been the limit. Pure hydrogen start at reaction gas flow rate and 1 Torr. 400 V/0.5 A (current limited) used to initiate the discharge. The main evacuation valve was closed, and a computer controlled bypass needle raised the pressure and power simultaneously to reaction conditions. This was then held for 2-4 mins.	Evacuated to 0.001 Torr. Discharge chamber was initiated and the power and pressure "were gradually increased up to deposition conditions". No specific gas % given but methane is 0 and slowly bled in after the stabilization of the plasma, with no time given. Reaction gas flow rate presumed (150).		H only plasma was stabilized at deposition conditions before Me was introduced. Current limited so a V increase of ~20 V was seen, but doesn't state if starting or final voltage given.	No information given.	Evacuated to ~10-4 Pa. H introduced to 26600 Pa and V applied to start discharge. Substrate heated to 850 °C then deposition conditions were initiated. 100sccm of pure H presumed.
CH ₄ conc. / Vol %	4	5	0.5	7	?	2
H ₂ conc. / Vol %	96	94.5	6	93	?	98
Ar conc. / Vol %	0	0	88.5	0	?	0
N ₂ conc. / %	0	0.5	5	0	?	0
Combined Gas Flow Rate / sccm	300	150	150	400	200	100
Deposition Time / h	5	? (48 h for W)	?	?	?	?
Voltage / V	800	450	320	840±20	? (~40 kW power)	?
Current / A	4.5	45	0	89	?	? (4 A/cm ² current density)
Pulse/Pause / μs/μs OR Pulse Frequency / kHz	72/50	DC	DC	DC	DC	DC
Anode/Cathode separation / mm	25	5	5	Few centimeters.		~2
Substrate temperature / °C	950-1050	750-850	750-850	1200-1300	?	850 presumed
Cathod Temperature / °C	900-1000	750-800	750-800	?	?	?
Pressure / Torr	200.26	110-150	110-150	100	150	
Cool Down	After the run time the methane gas flow was halted and the discharge continues for a further 5 minutes in just hydrogen.	No cool down notes given.		"cooled to room temperature"	No cool down notes given	
Notes	"In the case of disturbances, such as discharge breakdown or parts of the layer chipping off, the computer restarted automatically." Mo substrate and cathode (20 mm φ), grounded anode, powered cathode.	4 inch Si wafer for deposition, W cathode. W has no lit. ref. to reaction with H ₂ or N ₂ so thought very stable. Ultrasonically seeded the Si wafer with ~3 nm diamond powder in methanol.		8 in Mo substrate. Anode and chamber wall grounded. Cathode given negative voltage.	4 inch wafer. Cathode (Mo) connected to power, grounded anode (W). Multiple runs done but no specifics to certain runs were presented.	<1 cm substrate diameter
Diamond Quality	Very even thickness but diamond overgrown the edges. Peak growth rate of 41 μm/h. <110> preferred growth.	W cathode was exceptionally stable, producing smooth and clear diamond coating. 0.4 μm/h calculated by me. Grain size below 10 nm.		Very uniform, smooth diamond. 7~9 μm/h growth rate. Minimal wafer thickness, crystallinity, and thermal conductivity variation.	Max 19 μm/h growth rate observed.	20 μm/h growth rate.
Fabrication Notes	Problems with adhesion to Molybdenum, cathode temperature for successful deposition 900 - 1000 C (lower gave carbon deposits, higher gave thick carbide layer, both affected discharge), PS pulse/pause rate & parallel cathode/substrate both important for stable discharge, PS pulse matched to gas composition, shorter pulses for lower methane concentration and discussion of ns pulses being useful, discussion of plasma shape, color, deposition provide & size of electrodes			Instability in medium pressure range 100~150 Torr, diamond wafer just falls off Mo substrate after cooling.		